Fall 2007

Oblique Photogrammetric Analysis of Dome Growth at Mount St. Helens Volcano, 2004 – 2007

Angela K. Diefenbach
Western Washington University

Follow this and additional works at: https://cedar.wwu.edu/wwuet

Part of the Geology Commons

OBLIQUE PHOTOGRAMMETRIC ANALYSIS OF DOME GROWTH AT MOUNT ST. HELENS VOLCANO, 2004-2007

BY

ANGELA K. DIEFENBACH

Accepted in Partial Completion

of the Requirements for the Degree

Master of Science
Geology

_____
Moheb A. Ghali, Dean of the Graduate School

ADVISORY COMMITTEE

_____
Chair, Dr. Juliet G. Crider

_____
Dr. Daniel Dzurisin

_____
Dr. Jackie Caplan-Auerbach

_____
Dr. Scott Linneman

MASTER'S THESIS

In presenting this thesis in partial fulfillment of the requirements for a master's degree at Western Washington University, I grant to Western Washington University the non-exclusive royalty-free right to archive, reproduce, distribute, and display the thesis in any and all forms, including electronic format, via any digital library mechanisms maintained by WWU.

I represent and warrant this is my original work and does not infringe or violate any rights of others. I warrant that I have obtained written permissions from the owner of any third party copyrighted material included in these files.

I acknowledge that I retain ownership rights to the copyright of this work, including but not limited to the right to use all or part of this work in future works, such as articles or books.

Library users are granted permission for individual, research and non-commercial reproduction of this work for educational purposes only. Any further digital posting of this document requires specific permission from the author.

Any copying or publication of this thesis for commercial purposes, or for financial gain, is not allowed without my written permission.

Name: _Angela Dieffenbach_

Signature: _____

Date: _7/19/18_

MASTER'S THESIS

In presenting this thesis in partial fulfillment of the requirements for a master's degree at Western Washington University, I agree that the Library shall make its copies freely available for inspection. I further agree that copying of this thesis in whole or in part is allowable only for scholarly purposes. It is understood, however, that any copying or publication of this thesis for commercial purposes, or for financial gain, shall not be allowed without my written permission.

Signature _____

Date ___11/8/2007___

OBLIQUE PHOTOGRAMMETRIC ANALYSIS OF DOME GROWTH AT MOUNT ST. HELENS VOLCANO, 2004-2007

A Thesis
Presented to
The faculty of
Western Washington University

In Partial Fulfillment
of the Requirements for the Degree
Master of Science

By
Angela K. Diefenbach
November, 2007

ABSTRACT

This project is an oblique photogrammetric survey of the 2004-2007 dome-building eruption of Mount St. Helens volcano with two primary objectives: (1) to evaluate the potential of a new rapid and low-cost technique to create digital elevation models (DEMs) and subsequently calculate dome volumes and extrusion rates at Mount St. Helens; and (2) to attempt to understand mechanics associated with lava dome extrusion and collapse by analyzing volumetric and extrusion rate measurements in the context of dome height measurements, seismicity data, and migration of the locus of dome growth.

The new method uses sets of oblique aerial photographs, acquired from a helicopter with a standard digital camera, and commercially available photogrammetry software to create DEMs. Twelve sets of overlapping digital images from November 2004 to April 2007 of the growing dome inside the crater of Mount St. Helens were used to produce DEMs. Analyses of the digital images were carried out using PhotoModeler software, which produces three dimensional coordinates of points identified in multiple photos.

The DEMs were used for qualitative and quantitative descriptions of the 2004-2007 eruption. The DEMs were used to calculate height, volume, and extrusion rate, and to track changes in these quantities through time. These quantities show a decreasing extrusion rate through time that has remained lower than 1 m^3/s since October 2005. Total dome volume had reached 94×10^6 m^3 as of April 2007, a larger volume than that of the 1980-1986 Dome. Quantitative evaluation of the DEMs also shows a relationship between dome height and extrusion rate, which varies with the character of eruptive activity.

Results were validated by comparing volume measurements derived from traditional aerophotogrammetric surveys run by the USGS Cascades Volcano Observatory. The new oblique photogrammetric technique yields estimates of eruptive volume consistently within 5% of the volumes estimated with traditional surveys. The end result of this project is a new technique that provides inexpensive, rapid assessment of volcanic activity that can be an important supplement to volcano monitoring worldwide.

ACKNOWLEDGEMENTS

TABLE OF CONTENTS

LIST OF FIGURES

LIST OF TABLES

1. INTRODUCTION

Rapid analysis of volcanic activity during periods of unrest and eruption is very important for event monitoring, prediction, and disaster mitigation. One of the main techniques used to monitor volcanic activity involves the measurement of surface deformation (e.g. Dzurisin, 2000). Deformation of the Earth's surface at a volcanic edifice is commonly a precursor to volcanic activity. During an eruption, deformation measurements can provide important information about the size and potential impact of future eruptive activity. Surface deformation can also be measured post-eruption, sometimes in the form of subsidence from cooling and compaction of lavas. Overall, the measurement of changes in a volcano's surface is key to understanding eruptive dynamics and can be used to reduce or mitigate volcanic hazards.

The most essential measurement of surface change during a volcanic eruption is the volume and associated extrusion rate of lava, a measurement that can be used to calculate the energy of an eruption (Herd et al., 2005; Wadge et al., 2006). Measurement of the volume of lava and the rate at which lava emerges from a volcano are fundamental properties of the dynamics of volcanic eruptions. These measurements are used to constrain models of eruption dynamics produced by other monitoring techniques such as gas, geochemistry, seismicity and geodesy (Wadge, 2003; Stevens, 2002). The volume of lava extruded, in the form of flows or domes, is necessary to give an accurate indication of the amount of magma a volcanic system is capable of holding, which provides insight into magma storage, the plumbing system and eruption duration (e.g. Stevens, 2002; Harris et al., 2003; Kaneko et al., 2002).

A traditional technique used to measure eruption volume is photogrammetry. Photogrammetry is the science of obtaining quantitative measurements from photographs (American Society for Photogrammetry and Remote Sensing, 2006). In the last few decades, with advances in computer systems and software, photogrammetry has moved from analogue to digital format. In volcano monitoring, this has immense advantages because digital photogrammetry can allow for near-real-time, precise measurements of both broad-scale and local surface change (e.g. Honda and Nagai, 2002; Bluth and Rose, 2004).

This manuscript describes a photogrammetric study of Mount St. Helens volcano in southwestern Washington. Recent activity at Mount St. Helens provides a rare opportunity to devise and test methods for better understanding and predicting volcanic events by making observations at an accessible, thoroughly studied and well-instrumented volcano. This study seeks to measure volcanic activity at Mount St. Helens by calculating the volume of the growing dome and simultaneously test and evaluate a new technique in volcano monitoring. The new technique is a low-cost form of photogrammetry, using an off-the-shelf digital camera, commercially available software and a laptop computer to rapidly produce three dimensional images of the extruded lava at Mount St. Helens, at several dates spanning two years. The sequence of images is used to estimate eruption volumes and time-averaged extrusion rates. The end result of this project is a new technique that provides inexpensive, rapid assessment of volcanic activity that can be an important supplement to volcano monitoring worldwide.

1.1. Volcano Monitoring Tools

Scientists monitor volcanoes for two reasons: (1) to assess hazards by monitoring the level of volcanic unrest; and (2) to understand eruption mechanisms and physical processes occurring within a volcano, such as magma migration (Dzurisin, 2006; Scarpa and Tilling, 1996). Surface deformation is a primary measurement of volcanic unrest and is also used to better understand eruption dynamics. Tools used to monitor surface deformation range from hand-held leveling rods to satellites in space (e.g. Dzurisin et al., 1999; Pederson and Sigmundsson, 2004; Yokoyama and Seino, 2000). Advances in technology have made possible numerous ways of collecting spectral, spatial and temporal data, from land and from space, that are useful for researching active volcanoes. Techniques used to monitor surface deformation can be put into one of two categories: (1) point-based measurements and (2) synoptic imagery (Cecchi et al, 2003). Table 1 gives a summary description of these tools and techniques employed in volcano monitoring.

Traditional techniques used to monitor surface deformation in volcanic areas involve the use of geodetic equipment such as spirit levels, Global Positioning System (GPS) receivers, electronic distance meters (EDM), tiltmeters and strainmeters (Poland et al., 2006b; Dzurisin, 2006). These techniques can measure surface displacements with accuracies in the decimeter range or better, but often can be expensive and allow only scarce (few tens to a few hundreds) sampling of data points within the deformation field. This limited sampling can fail to record localized or complex deformation occurring on the volcano. Another disadvantage to these traditional techniques is that they cannot be individually used to determine the volume of a growing dome or lava flow, without

3

making, for example, a sufficient number of EDM or GPS measurements to adequately characterize the changing shape of the dome (logistically very difficult).

In the last decade, remote sensing has become an advantageous tool for measuring surface deformation on volcanoes because of its broad spatial coverage and relatively low cost. Interferometric Synthetic Aperature Radar (InSAR) has led the way in satellite remote sensing (Coulson, 1996; Poland et al., 2006a; Lu et al., 2002; Dzurisin et al., 2006). Unfortunately SAR data are limited by the periodicity of satellite passes over a given area (35 days with ERS satellites) and environmental conditions such as steep slopes, vegetation, ice cover, and weather; problems often associated with volcanoes (Baldi, et al., 2002). Light Detection And Ranging (LiDAR) is a relatively new remote sensing technique that can provide very high resolution, three-dimensional models of volcanoes from laser return signals, but is often too expensive to have widespread application at this time (e.g. Pyle and Elliott, 2006).

Table 1. Volcano monitoring tools used to measure surface deformation.*

Methods	Scientific Target	Instrumentation
Point based techniques		
Space geodesy	Far- and near-field point displacements	Dual and single frequency GPS
Tilt measurements	Angle variations	Dry-tilt, wet-tilt, borehole tiltmeters
Leveling	Vertical component displacements	Theodolite, leveling rod
Electron Distance Meter (EDM)	Far-field point displacements	Transmitter-receiver, reflectors, tape, callipers
Image techniques		
Photogrammetry -airborne -groundbased	Volume measurements	Analogue and digital cameras (metric and non-metric types of both)
LiDAR -airborne -groundbased	Volume measurements	Laser
Radar Interferometry	Volume measurements	ERS1-2, RADARSAT, TOPSAR, SIR

*Adapted from Cecchi et al., 2003 and Poland et al., 2006b.

Another branch of remote sensing that has been used for several decades to evaluate volcanic activity is photogrammetry. Photogrammetry derives three-dimensional spatial information from imagery, typically photographs. Dependent on the type of survey conducted, photogrammetry can be cost effective, have various degrees of spatial and temporal resolution, and provide accurate and precise measurements of volcanic growth. The application of photogrammetry within volcanology has generally been confined to the construction of digital elevation models (DEMs) from vertical air photos (e.g. Baldi et al., 2000) to produce topographic models and to constrain volumes of volcanoes. Recent advances in digital imagery and software have expanded the capabilities of photogrammetry, now making it possible to measure extrusion rates and

map lava flows (e.g., Wright et al., 2002; Harris et al., 2000). Photogrammetry has also been used for comprehensive laboratory analogue studies of volcanic systems (e.g., Fink and Bridges, 1995).

1.2. Geologic setting

Mount St. Helens is a young composite volcano centrally located along the north-south transect of the Cascade Volcanic Range, which stretches from British Columbia to northern California (Fig. 1). Subduction of the Juan de Fuca plate below the North America plate is the driving force behind volcanism in the Cascades. Mount St. Helens has long been the most active and explosive stratovolcano in the Cascade Range, building its edifice with the production of lava domes, predominantly dacitic in composition (Pallister et al., 1992; Sherrod and Smith, 1990; Clynne et al., 2005). Intermittent explosive behavior has characterized Mount St. Helens since about 300,000 years ago (Mullineaux and Crandell, 1981; Clynne et al., 2005). Four stages of volcanic activity (Ape Canyon, Cougar, Swift Creek and Spirit Lake) separated by dormant intervals characterize the complex geologic history of Mount St. Helens (Clynne et al., 2005). During the past 2,500 years, at least half a dozen dacitic lava domes have formed at Mount St. Helens, including the Goat Rocks dome that formed on the volcano's north flank during an eruption from 1800 to 1857 (Moore et al., 1981).

1.2.1. Eruptive activity of Mount St. Helens: 1980-1990

Field investigations in the 1970's (Crandell et al., 1975) led researchers to believe that the violent history of Mount St. Helens rendered this volcano the most dangerous and

6

frequently active in the Cascade Range. On May 18, 1980, following two months of unrest, Mount St. Helens erupted explosively with a lateral blast, leaving a horseshoe crater roughly 2 kilometers wide (Fig. 1B). Mount St. Helens continued to have episodes of moderately explosive activity and dome growth through 1986 (Swanson and Holcomb, 1989). The eruptions of May 25, June 12, July 22, August 15, and October 12, 1980 were moderately explosive, while from December 1980 to October 1986, eruptive activity was dominantly extrusive in character (Swanson and Holcomb, 1989). Periods of dome growth lasted from 1 to 24 days, plus an anomalous growth period that lasted most of 1983 (Swanson and Holcomb, 1989). October 1986 marked the last episode of dome growth in the 1980s at Mount St. Helens. During more than seventeen episodes of dome growth, Mount St. Helens grew a composite dacite lava dome with a volume of 92×10^6 m^3 as calculated by vertical aerophotogrammetry and digital topographic maps (Thompson and Schilling, 2007; Mills, 1992). In 1989 Mount St. Helens experienced an increase in seismicity followed by a small series of minor phreatic eruptions in January and November 1990 (Pallister et al., 1992) but no new lava emplacement occurred. No juvenile material reached the surface during this episode, which was followed by nearly 14 years of repose punctuated by sporadic swarms of small earthquakes (Moran, 1994).

Following the May 18, 1980 eruption, a glacier (Crater Glacier) formed within the crater of Mount St. Helens. September 2001 vertical aerial photography estimated the glacier to have a maximum thickness of 200 m and contained 120×10^6 m^3 of ice and rock debris (Schilling et al., 2004).

1.2.2. *Eruptive activity of Mount St. Helens: 2004-2007*

In October 2004, Mount St. Helens began erupting new dacite lava after nearly 18 years of eruptive quiescence. Early stages (October 2004 - December 2004) of the eruption were characterized by lineal (two-dimensional measurement derived by stationary cameras and spider GPS stations) lava extrusion rates of 6-11 m/d and volumetric (three-dimensional measurement derived by photogrammetry) extrusion rates of 4-6 m^3/s (Dzurisin et al., 2005). Following this rapid flux of new dacite, the volcano continued a relatively steady lineal extrusion rate of 2-3 m/d for nearly 14 months; since that time, the rate has declined to less than 1 m/d and growth has become mostly endogenous. Corresponding volumetric rates are 1-3 m^3/d and about 0.7 m^3/d. Two and a half years of dome building has resulted in the emplacement of roughly 9.3×10^7 m^3 of new lava on the crater floor (Table 2). By spring 2007, the new lava dome volume was greater than that of the 1980-1986 lava Dome, and the average 2004-2007 growth rate was nearly three times that of the 1980-1986 Dome.

Table 2. Total volume change, extruded lava volume, and rates of change during the 2004-2007 eruption of Mount St. Helens as measured by vertical aerial photogrammetry (vertical aerophotogrammetry)*

Date of vertical aerial photography	Total extruded lava (x 10^6 m³)	Lava extrusion rate (m³/s)
11/4/2004	12	5.92
11/29/2004	21	4.40
12/11/2004	26	4.05
1/3/2005	31	2.52
2/1/2005	35	1.84
2/21/2005	39	2.37
3/10/2005	42	1.84
4/19/2005	48	1.62
6/15/2005	54	1.30
7/14/2005	57	1.28
8/10/2005	62	1.97
9/20/2005	67	1.58
10/24/2005	70	0.92
12/15/2005	73	0.67
2/9/2006	77	0.87
4/18/2006	81	0.65
8/18/2006	85	0.40
10/21/2006	88	0.45
12/6/2006	90	0.45
4/20/2007	93	0.27

* From Schilling et al., *in press*; S. Schilling, personal communication, July 3, 2007.

1.3. Previous work in photogrammetry

Photogrammetric surveys have been conducted at volcanoes worldwide for several decades. These surveys have varied in technique, resolution, and precision and have been used in conjunction with other volcano monitoring tools to better understand eruption dynamics and volcanic hazards. The purpose of this section is to summarize the use of photogrammetry to monitor volcanoes worldwide and to describe different

photogrammetric techniques that have been employed at Mount St. Helens since the cataclysmic eruption of May 18, 1980.

1.3.1. Previous work using photogrammetry to study volcanoes

The main products of photogrammetric surveys are digital elevation models (DEMs) that may be used to measure volume and to calculate extrusion rate at a volcano. Comparison of sets of DEMs constructed from photos taken on different dates can be used to study and monitor several geophysical processes at volcanoes involving crustal deformation and extrusion of lava. These include deformation patterns, displacement vectors, volumes and extrusion rates and other physical features, providing quantitative information on the geomorphic evolution of a volcano (e.g. Schilling et al., *in press*; Achilli et al., 1997; Kaab and Funk, 1999; Baldi et al., 2000; Kerle, 2002; Pyle and Elliott, 2006; Wadge et al., 2006). The quantitative information extracted from DEMs can be used to describe and measure volcanic activity and can be used in conjunction with other datasets, such as gas emission rates, geochemistry of erupted products (gas, ash, or lava), and geodetic measurements, to model volcanic processes.

Most photogrammetric surveys conducted at volcanoes are completed to produce a topographic map or a three-dimensional base model of the volcano in the form of a DEM. These surveys are done by means of a low-flying aircraft, capturing vertical aerial photographs of the edifice and surrounding landscape (e.g. Schilling et al., in press; Baldi et al., 2002; Chandler and Moore, 1989). Recent advances in computer hardware and software has expanded photogrammetry from analogue to digital. Baldi et al. (2000) and Miranda and Granados (2003) have successfully monitored landslides and glaciers on

10

volcanoes for hazard mitigation purposes. Surveys by James et al. (2006) employed

terrestrial photogrammetry to measure and monitor active lava flows and reference

topographic models with thermal imagery. Herd et al. (2005) used terrestrial

photogrammetry to build DEMs of Soufriere Hills Volcano to measure collapse-scar

volumes. Oblique images have been used to determine rapid changes in volcano

topography from image sequence matching, comparing volcano profiles through time to

determine two-dimensional change (Cecchi et al., 2003). The use of photogrammetry

within volcanology has grown, and researchers continue to experiment with the

capabilities photogrammetry has to offer in volcano monitoring.

1.3.2. Previous work at Mount St. Helens: 1980 - 2007

The use of photogrammetry for volcano monitoring at Mount St. Helens began

with a series of six topographic maps made by means of vertical aerial photography pre-

and-post the volcano's awakening in 1980 (Moore and Albee, 1981). Moore and Albee

(1981) used these maps to measure displacements on the volcano's deforming north flank

and to map the outline of extruded lava within the crater of Mount St. Helens. Jordan and

Kieffer (1981) calculated volume changes before and during the eruption by differencing

Digital Terrain Models (DTMs) produced from vertical aerial photographs taken in 1972

and numerous dates in 1980. During the dome-building eruptions from October 1980

through November 1986, several maps of the crater and dome were made from low-

altitude, high-resolution vertical aerial photographs. These maps proved very successful

in documenting the changing size and shape of the lava dome (Holcomb and Colony,

1995). Photogrammetric surveys continued after volcanic activity ceased in 1986 in

order to produce DEMs of the volcano. Aerial photographs taken in 1980, 1992 and 2000 were used to create 1:24,000 scale digital topographic maps, from which DEMs were constructed. The DEMs were used to track the growth of a new crater glacier and the amount of mass wasting of rock from the steep crater walls (Schilling et al., 2004).

In 2000, a network of ground control targets from campaign GPS receivers was deployed on the volcano's outer flanks to provide ground control for the production of a high-resolution, high-accuracy DEM of Mount St. Helens by means of aerotriangulation (a digital method used to tie ground control within a strip of photographs) (Thompson and Schilling, 2007). This photogrammetric survey proved vital with the onset of eruption at Mount St. Helens in 2004, because a network of control was already established enabling the production of successive high-resolution DEMs with minimal preparation. Seventeen DEMs were constructed between 2004 and 2005 to measure volume change and extrusion rate of the eruption (Schilling et al., *in press*), and the production of these DEMs is continuing on a quarterly basis.

Stationary, terrestrial photogrammetry has provided an effective, minimally invasive tool for assessing short-term, large scale changes at Mount St. Helens. At times (when field crews are absent), the permanent camera stations on the rim of Mount St. Helens provide the only visual insight into activity at the volcano (Poland et al., 2006). At present (September 2007), six permanent camera stations monitor the activity inside the crater of Mount St. Helens from the volcano's rim and outer floor. Photogrammetric techniques, utilizing daily photographs telemetered to the USGS Cascades Volcano Observatory have been used to analyze point changes (vector displacements) beginning at the onset of eruption in 2004 (Major et al., *in press*). Though this technique cannot

12

provide volumetric measurements, it has proven successful for measuring lineal extrusion rates (Major et al., *in press*).

The previous studies done at Mount St. Helens and elsewhere in the world have helped to identify the type of photogrammetric survey needed at active volcanoes, when traditional photogrammetric techniques prove too expensive, time-consuming or dangerous.

1.4. Thesis Motivation and Objectives

Over the last three decades, photogrammetry has been successfully used to monitor surface change at volcanoes and has yielded estimates of eruption volume, rate of extrusion, and vector displacements (Schilling et al., *in press*; Major et al., *in press*; Kerle, 2002; Moore and Albee, 1981; Zlotnicki et al., 1990). Advances in technology have allowed photogrammetry to evolve from analogue to digital format, thereby saving time and money. Even with the move from analog to digital data, traditional photogrammetric techniques continue to be relatively time-consuming and expensive. Agencies must contract aerial flight services, be equipped with stereoplotters and high-resolution scanners, and employ an experienced technician to run the hardware and software necessary for extracting quantitative information from the photographs. The motivation behind this project is to develop a rapid and inexpensive method of calculating volume and extrusion rate. The goal is not to eliminate the need for traditional methods of photogrammetry, but to supplement these methods, or provide an alternative when funding is insufficient, equipment is not available, or hazards at the volcano prevent the use of traditional methods.

In this study, I have employed a new method for monitoring lava dome growth at Mount St. Helens with the following objectives: (1) to evaluate the potential of a new cost-effective technique to create DEMs and subsequently calculate dome volumes and extrusion rates at Mount St. Helens; and (2) to attempt to understand mechanics associated with lava dome extrusion and collapse by analyzing volumetric and extrusion rate measurements with results from seismicity data.

2. METHODS

2.1. Principles of Photogrammetry

Photogrammetry is the science of obtaining three-dimensional spatial information from two-dimensional images. Photogrammetry has been used in the geologic sciences for many years, most notably for the production of topographic maps and digital elevation models from overlapping aerial photographs (e.g. Chandler, 1999; Lane et al., 2000; Baldi et al., 2000). Recent advances in photogrammetric software now allow the use of consumer grade digital cameras to provide quantitative photogrammetric analyses, making this technique easily accessible by many disciplines ranging from forensic sciences to archaeology (e.g. Lynnerup and Vedel, 2005; Heinz, 2002). Independent of the size or type of study, photogrammetry relies on the same basic principle of triangulation, a means by which three-dimensional point measurements are produced using collinearity equations. The concept of collinearity, whereby a point on the object, center of lens and resultant image point lie on a single line in three-dimensional space, is critical in photogrammetry (Mikhail et al., 2001). Based on this principle, the three-dimensional object space coordinates can be extracted from a pair (or series) of overlapping photographs, provided that interior and exterior orientation of the camera at the moment of exposure are known. Exterior orientation parameters of the camera can easily be determined with the help of a minimum of three ground control points (GCPs) for each image (Wolf and Dewitt, 2000). Interior orientation parameters of the camera are determined using a "self-calibrating bundle adjustment" (see below). The morphology of the object under study is derived from pure photogrammetric information;

15

its volume and geographic location are obtained from the additional internal and external orientation information given into the object space (the three-dimensional region that encompasses the physical features imaged in the photographs) (Wolf and Dewitt, 2000).

I use oblique photogrammetry to study the growing dome of Mount St. Helens volcano, capturing images by means of digital photography from a helicopter. Oblique photogrammetry differs from traditional aerial photogrammetry in that the camera system captures images inclined from the vertical axis. Oblique photogrammetry uses the same mathematical principles as vertical photogrammetry, proceeding in steps going from image acquisition, to camera calibration, to relative and absolute image orientation and finally image analysis and DEM construction.

2.2. Data Acquisition

Images were acquired during helicopter flights run by the USGS Cascades Volcano Observatory. Twelve sets of photographs were taken between November 2004 and April 2007, with each date referred to as an "epoch". Helicopter flights were scheduled on the same day as vertical aerial photograph flights to provide direct quantitative comparison to traditional photogrammetric techniques for measuring dome growth through the eruption. Low-altitude oblique helicopter images provide an advantage over traditional aerial photographs during times of inclement weather (low cloud cover) and persistent steaming, in that they provide oblique views of the dome that minimize obstruction from atmospheric affects. Images were taken with a Nikon D70 digital SLR camera, with a 6.1 megapixel sensor (Fig. 2). An NF 17-55mm Nikkor lens was used with lens focal length set to infinity to provide the widest view angle and to

maintain consistency while acquiring images. Images were shot in RAW format and later converted to JPEG using Nikon Image Capture software; this process provides an image with a slightly sharper appearance and a little more contrast than images captured directly in JPEG format. All images were taken in landscape view with an average of 60% longitudinal overlap (common area captured), to enable tie point measurement and to allow a common processing of all images in a bundle adjustment. Helicopter flights followed a square path over the volcano as viewed from above, increasing in altitude for every repeat circuit (Fig. 3). This technique provided several sets of photographs for each epoch that could be chosen for processing, dependent on operator needs. Low-altitude flights provided close-range views of features on the dome, while higher altitude flights encompassed views of the crater wall and rim and 1980-1986 Dome used for GCPs and reference points during processing.

2.3. Camera Calibration

Another important step is camera calibration. In photogrammetry, there are two types of cameras; metric and non-metric. Metric cameras have stable and precisely known internal geometries. Because this project used a standard off-the-shelf digital camera (non-metric), for purposes of ease and low-cost, internal camera geometries are unknown. In order to complete a photogrammetric analysis of the images acquired, accurate calibration of the camera and lens is necessary. Calibration must be done in a 3D reference frame and in the same conditions as operational use in the field, in this case, with focus set to infinity. The Nikon D70 camera was calibrated by means of the camera calibrator, a built-in extension of the PhotoModeler software (PhotoModeler, 2005).

Calibration can be done before or after fieldwork and was required in order to determine the camera's interior (camera type) and exterior (camera location) orientation. In this numerical procedure, the interior and exterior parameters of all frames are simultaneously estimated using a least squares estimation (Wolf and Dewitt, 2000). The main parameters of interior orientation are the principal point (intersection of the image plane and the principal ray normal to the image plane), principal distance (focal length), sensor format size, and lens distortion characteristics.

The calibration was done using the standard procedure from the PhotoModeler user manual. PhotoModeler software provides a simple procedure for estimating these values by analyzing a grid target. A target grid provided by PhotoModeler was projected onto a wall using a slide projector. The grid comprises 100 uniformly spaced black dots, aligned in columns and rows, with four of the dots on the outer edges outlined by symbols, representing control points within the target (Fig. 4). The target was photographed from four camera locations. At each location, a photograph was taken in landscape view and then the camera was rotated 90 degrees and a portrait view was taken. Images were input into PhotoModeler's calibration extension and camera interior orientation parameters were estimated. PhotoModeler automatically processes the images and reports the characteristics of the camera. PhotoModeler provides an output text file that estimates overall calibration performance and object accuracy represented by average root mean square (RMS) residuals discussed in the error estimation section of this thesis. The calibration adjustment was performed successfully for all sets of photographs, with acceptable residuals of the control points. According to the PhotoModeler documentation, a project with a good calibration has a final error under

0.15 and marking residual error under 1.0 pixels. Camera calibration for the Nikon D70 produced a final error of 0.077 and an overall RMS or marking residual of 0.311 pixels. Given these calibration checks, the Nikon D70 calibration file provides a quantitatively accurate description of the camera interior orientation parameters necessary for a successful project.

A benefit of using PhotoModeler is that the user does not need to measure the exterior orientation (camera location parameters) during image acquisition. PhotoModeler automatically calculates the three spatial coordinates and the three orientation angles of each camera, or each camera position at which an image is taken, assuming reference points and GCPs (approximately 10 total) are used in the overlapping photographs. This process is known as resection (Mikhail et al., 2001). Knowledge of the camera's interior and exterior orientations made it possible to process three dimensional models of the growing dome inside the crater of Mount St. Helens without having to measure the coordinates of the camera in the moving helicopter at the instant each photo was taken. It is possible by using GPS tracking, either of the helicopter or of the camera itself with GPS hot-shoe attachments that are available for a few modern digital cameras, to acquire exterior orientation information independently, but for this work it was not necessary and therefore GPS tracking was not explored.

2.4. Image Processing

For each epoch, 4 to 7 images were used. The images were chosen based on percentage of overlap, optimum angle of convergence (i.e. the angle of difference between camera positions, at the time of image acquisition, relative to one another) and

area of the dome captured. In photogrammetry the optimum angle between camera stations is between 45 to 90 degrees. The lowest acceptable angle of convergence is 20 degrees (PhotoModeler, 2005).

2.4.1. *Image Orientation*

Generation of a 3D model requires knowledge of the relative and absolute orientation of the images as well as measurement of the positions of points in each image. Relative orientation means the determination of the projective centers of the images in an arbitrary spatial coordinate system by measurement of at least 6 homologous points (tie points). Absolute orientation means their orientation in a Cartesian coordinate system, which can be achieved by measurement of a minimum of 3 control points (points with known spatial coordinates) (Mikhail et al., 2001). Once control points and tie points are selected and orientations set, PhotoModeler produces a bundle block adjustment to process each project, resulting in an accurately referenced three-dimensional model of the study area. The term bundle block adjustment refers to the method of orienting and processing a block of images, simultaneously, that cover the area of interest in the study.

2.4.2. *Relative Orientation*

Oblique photographs were taken on twelve dates, between November 2004 and April 2007. The processing for each epoch of photographs is considered a project. Each project consisted of 4-7 photographs. In order to tie the photographs together in arbitrary space and give the three-dimensional model correct, relative dimensions, approximately 6-7 tie points need to be selected and identified in all images. For the purpose of this

20

study, tie points are those points residing in every image involved in a project, that tie images together for relative orientation. Tie points differ from reference points in that the latter are shared between two or more images and are not required to be seen in every image. On the other hand, each tie point must be seen in every photograph of the project. This step is the most time consuming because varying camera locations and angles can make identifying corresponding points in photographs difficult. Once tie points have been selected in each image, they are referenced using the reference tool in PhotoModeler. This process identifies the same tie points throughout a series of photographs.

2.4.3. Absolute Orientation – Control Methods

In order to construct a three-dimensional model from images it is essential to know the relationship between each image and the reference Cartesian coordinate system. Once imagery is acquired, ground control points (GCPs) must be identified and measured to tie the model into geographic space. A minimum of two planimetric and three height points are needed to define a datum (geographic coordinate system), but more control points are desirable to lower overall project error by increasing accuracy and precision. Ideal controls are points tying frames together and surrounding the volume of interest (Wolf and Dewitt, 2000). The use of GCPs located in the field by differential GPS provides the highest accuracy for control within a project compared to other methods, i.e. topographic maps, EDM measurements and DEMs. Schilling et al., (*in press*) established a network of GCPs from GPS stations at Mount St. Helens for vertical aerophotogrammetry, and CVO scientists deployed campaign GPS spiders (helicopter

21

deployable GPS units) on the growing dome and deforming glacier to establish positions and monitor deformation at the time oblique photography was taken. Unfortunately, few sets of oblique photographs contained visible GPS stations. For consistency between photo sets, I decided not to use GPS stations for ground control. Suitable control points for this project were well-defined natural features, clearly identifiable on the photographs and on independently-created high-resolution DEMs (2 m) (Fig. 5). Three-dimensional coordinates of these natural features were extracted from the DEMs. GCPs were prominent stationary features; three located on the crater rim and one the 1980-1986 Dome. The same four GCPs were used in each project to provide consistency and to accurately define the datum. Control points were evenly distributed over the images to gain a strong geometry.

Once relative and absolute orientation points were added in each project, the project was processed and PhotoModeler produced an accurately oriented three-dimensional model of the tie and control points within the photographs for each epoch. The next step involved the construction of a surface model, also known as a digital elevation model (DEM), for each epoch with reference points covering the 2004 – 2007 dome.

2.5. Digital Elevation Model (DEM) Construction

Once each project was oriented with tie and control points, reference points (selection of identical points between image pairs) were added to make models of the dome during successive epochs. This process was completely manual in that I (the operator) selected identical points on numerous images (minimum of two images for each

point) that encompassed the area of interest. Measurement and referencing between photos is done manually with the help of epipolar lines or auto-drive referencing (a form of semi-automated referencing) (Fig. 6). In this mode, when the source and destination images are oriented, the cursor and image will automatically jump to the expected location of the point in the destination image, allowing the execution of the final measurement to be done manually with a certain amount of aid provided by PhotoModeler.

The reference points were noticeable features, i.e. intersection of cracks on the 2004 – 2007 dome, edges of large talus and striae (Fig. 7). Placing reference points on the dome to construct DEMs of the evolving dome using PhotoModeler involved two steps: (1) reference points were identified that outlined the perimeter of the area of interest (Fig. 8A), (2) point clouds were created that filled in the area of interest (Fig. 8B).

The area of interest in each epoch was the growing dome inside the crater of Mount St. Helens volcano. In order to successively account for the material erupted between epochs, a perimeter of extruded rock was outlined with reference points throughout images. These perimeters account for all extruded rock throughout the eruption. The next step involved filling in that perimeter with a dense point cloud. As the density of points within the perimeter of the dome increased, so did the accuracy of representation of the dome's surface. In order to qualitatively depict the accuracy of the surface model created from reference points, PhotoModeler has a 3D viewer that allows the operator to select and delete significant outliers in the model as well as pinpoint areas that need an increase in point density.

The number of reference points and photographs used in each DEM varied (Table 3). DEMs with high point densities were the result of one or more of the following four conditions: (1) low flying altitude when photographs were taken, resulting in a higher pixel resolution, which facilitated identification of common points, (2) at the date the photographs were taken, the dome had more complex topography, requiring more points to accurately model it, (3) atmospheric interference (steaming at the vent) was minimal, exposing the entire dome, or (4) photographs captured the entire growing dome.

Table 3. Dates of oblique photography with associated number of points (GCP, tie and reference) and photographs used to build each DEM.

Date of oblique photography	Number of points used in model	Number of photographs used in model
11/20/2004	212	6
11/29/2004	412	7
01/03/2005	284	5
02/01/2005	566	7
02/22/2005	603	6
03/11/2005	484	6
04/10/2005	993	6
05/12/2005	1795	7
06/15/2005	798	7
10/12/2005	580	5
05/30/2006	415	5
04/20/2007	380	4

2.5.1. Delaunay Triangulation

Reference points are stored in a point table in PhotoModeler. The location of each point is stored as x, y, z (easting, northing, elevation) coordinate in North American Datum 1983 (NAD83), Universal Transverse Mercator (UTM), projection zone 10. This is directly related to the datum in which control points are cast. PhotoModeler allows the

operator to export the point table as an ASCII text file, which may be imported into ArcInfo Geographic Information System (GIS) as features. Using the 3D Analyst extension in ArcMap, the vector data points were used to create a Triangulated Irregular Network (TIN) for each epoch. Using the 3D Analyst menu and choosing the Create/Modify TIN - Create TIN from Features tool, each feature was converted into a TIN. A TIN is formed by nodes, triangles and edges from the computation of a Delaunay triangulation. Nodes are locations defined by x, y and z vector data values from which a TIN is constructed. Triangles are formed by connecting each node with its neighbors according to the Delaunay criterion: all sample points are connected with their two nearest neighbors to form triangles (Wolf and Dewitt, 2000) (Fig. 9). These triangles have sides that are as similar in length as possible to prevent the creation of long, narrow triangles that detract from the accuracy and visual appearance of the surface model (Hooper and Mattioli, 2001). A Delaunay triangulation converts the cloud of points extracted by photogrammetric procedures into a consistent polygonal model or mesh (Remondino and El-Hakim, 2006). These meshes have benefits when modeling complex terrains, such as that of Mount St. Helens, because they can be constructed to be more or less detailed depending on topographic complexity and can efficiently store data (Wolf and Dewitt, 2000).

2.6. Volume Calculations

To calculate volumes of the growing dome for each epoch as accurately as possible, it was necessary to use a pre-eruptive surface as a base. The first epoch of this study occurred after the onset of eruption at Mount St. Helens in October 2004, and thus I

25

did not have photographs of a basal surface to create a DEM of pre-eruption crater floor topography to use as a base for volume measurements. One way to calculate volume from a DEM is to use the lowest point of each DEM or set a low elevation point and extrapolate that point as a flat plane to use as a basal surface (Fig. 10A). This method of volume calculation, applied to the DEMs made of the 2004-2007 dome at Mount St. Helens, yields volume estimates that are significantly lower than the true volume of the dome, because it does not take into account the amount of extruded lava masked by the crater glacier, the varying topography of the crater surface since the last eruption, or the area of newly erupted lava that encroaches upon the 1980-1986 Dome. To get around this dilemma, and provide continuity when computing volumes from epoch to epoch, a 2 m DEM derived from vertical aerial photogrammetry of Mount St. Helens in 1986 was used for volume calculations (Schilling et al., *in press*). The use of the 1986 crater floor as a basal surface made the calculations more accurate than using a flat plane in two ways: (1) it accounted for topographic variations of the basal surface, and (2) since lava first extruded at the 1986 surface, then through the glacier inside the crater, and finally to the present surface, accurate volume calculations need to take into account the entire volume of the new dome, including that between the 1986 and present-day crater surface.

Volume estimates were complicated by the presence of Crater Glacier through which the 2004-2007 lava dome has emerged. The distribution of extruded rock masked by the severely deformed glacier presents the biggest source of potential error when calculating extruded rock volumes. For consistency, volumes reported are conservative volume estimates made by projecting the perimeter of the visible extruded lava vertically downward to the 1986 crater surface, representative of pre-eruption and pre-glacier

topography. In essence, this produces a cylindrical-like subsurface of extruded rock used in calculating volumes (Fig. 10B).

In order for volume calculations to be made, TINs were converted to regular grid DEMs to match the 1986 DEM used as a base. This was done using the 3D analyst extension in ArcMap and the "Convert TIN to Raster" tool. Each Raster was set at a 2 m cell size to match the resolution of the 1986 and 2004-2007 DEM sequences (produced by the USGS by means of vertical aerophotogrammetry), which were used for volume calculations and comparison, respectively, as described in section 4 of this manuscript. The high resolution, i.e. small cell size, allows the raster DEM to store the original elevation data contained within each TIN. The final results of these procedures were 2 m DEMs of each epoch.

Volumes for each epoch were calculated in ArcInfo using an Arc Macro Language (AML) script (Appendix A; Schilling et al., *in press*). Before the scripts were run, a boundary shapefile, delineating the area or shape of extruded lava was made for each DEM. The volume calculation script subtracts one DEM from another (the 1986 DEM as base from oblique DEMs) using the boundary file to clip the area of interest in both DEMs and produces an isoline grid that stores values resulting from the subtraction or elevation difference between models. The script takes each value (z) in the isoline grid and multiplies it by the area of a single cell (4 m^2) to calculate a total volume difference within the cell between the two DEMs. The volume difference is written to a text file.

3. ERROR ESTIMATION

Assessment of error involved in terrain modeling is not always straightforward; this is especially true in the case of this project where traditional photogrammetric techniques are not employed. Sources of error are directly related to the design of the photogrammetric survey, which includes camera calibration, sensor resolution, flight parameters, ground control and image orientation (absolute and relative), as well as random factors which include atmospheric interference (i.e. steam, heat shimmer, cloud cover), operator blunder and the nature and complexity of terrain being modeled. Error sources in DEMs are complex and varied. The most appropriate method for producing a DEM is therefore dependent on the application, the size of the study area, the time available for DEM construction and the error tolerance of the specific project.

The accuracy of a photogrammetrically acquired DEM relative to the surface from which it was derived is a function of sensor resolution, distance to object, the ground control network and the precision of measurements in the image (Wolf and Dewitt, 2000). Unfortunately, comprehensive analysis of accuracy and error is not possible for the project because of software limitations and complexity of variables involved. However, an estimation of accuracy and error is attainable. This project also has the advantage that vertical aerophotogrammetric surveys (Schilling et al., *in press*) were conducted at Mount St. Helens through the time period of this study, typically on the same day as oblique flights, which allows for comparison between techniques, ultimately producing an estimated accuracy of the DEMs (and derived quantities) that I have produced. The first evaluation of DEM accuracy and overall project error comes from the software used to build the three-dimensional models, PhotoModeler. The

28

second section of error analysis comes from the comparison between techniques and their associated measurements. A full description of the latter is presented in the results section of this manuscript.

3.1. PhotoModeler Evaluation

Photogrammetric precision achieved in this project can be examined using exported data tables from PhotoModeler Pro software. Average point tightness and root mean square (RMS) error in both pixels and meters for each epoch are reported in Table 4. Tightness values represent measurements of the maximum distance between any pair of projected light rays from the images to the object point (PhotoModeler, 2005). RMS residuals represent the difference between where the operator marked a given point and where PhotoModeler expects this point to be located (in x, y, z space). The location sought by PhotoModeler is defined by the projection and control that the operator input into the model in the early stages of processing. Inherently, if the ground control used by the operator to orient the model has error, this error then gets carried on to the residuals of reference points that make up the model.

For this project, ground control was established by extracting control points from a 2 m DEM constructed by means of vertical aerophotogrammetry. This was a necessary step because sensor (camera) locations were unknown at the time of image acquisition and no previous ground control survey had been established for this project. This was in the truest sense, an 'on-the-fly' operation. Thus, DEM error can be no less than the error calculated when producing the 2 m DEM used for control. This error is an estimated 0.17 m RMS residual (Schilling et al., *in press*).

Table 4. Average point assessment of oblique DEMs derived from quality report created by PhotoModeler Pro v.5 software.

Date of oblique photography	Average point tightness (m)	Average RMS residual (pixels)	Average pixel size (m)	Average RMS residual (m)
11/20/2004	2.6	3.9	.20	.80
11/29/2004	1.9	2.3	.45	1.0
01/03/2005	4.5	2.4	.80	1.9
02/01/2005	2.2	2.8	.28	.80
02/22/2005	2.8	3.6	.42	1.5
03/11/2005	2.6	2.8	.80	2.2
04/10/2005	1.9	3.4	.67	2.3
05/12/2005	1.3	1.9	.30	.60
06/15/2005	1.6	2.3	.50	1.2
10/12/2005	1.5	1.5	.50	.75
05/30/2006	2.5	3.5	.50	1.8
04/20/2007	1.4	1.3	1.0	1.7

RMS residuals are one of the best indicators of project quality and should always be checked after processing. According to Wolf and Dewitt (2000) the term "error" is frequently used in photogrammetry when RMS residual is described, since errors are indeterminate. According to PhotoModeler (2005) all projects should have the largest RMS residual under 10 pixels. For projects with known and calibrated cameras the largest residual should be less than 3 pixels. For this project average RMS marking residual for all dates was 2.6 pixels.

The quality report that PhotoModeler exports assign RMS error in pixel units. In order to spatially understand the RMS residuals, a conversion from pixel units to meter units was necessary. The linear ground distance that a pixel represents in a photograph, also called ground sample distance (GSD), is a nontrivial calculation in highly oblique imagery. In fact, the difference in scale from foreground to background in an individual

photograph can be tens to hundreds of meters depending on obliquity and flying distance from object (Doneus, 2001). However, to produce an estimate of the precision of this technique in units useful to a geoscientist, I calculated an average GSD for the pixels in each DEM. To determine an average GSD for each model, I chose three pairs of points in each model. These points were chosen based on their location within each model (i.e. I chose points on the dome rather than ones used to tie the images together that may have been on the crater rim or glacier). Using the zoom tool in PhotoModeler, I was able to count pixels between points. Evaluation of the ID properties of each point gave the easting, northing and elevation data in meters. The difference between easting and northing of each point gave a distance (m) between points. Dividing the distance (m) by the number of pixels between points gave an estimation of the GSD of a pixel (Fig. 11). I used the average from the three point pairs to get an average GSD for each project. This average GSD (m) was then multiplied by the RMS in unit pixels to get an RMS in unit meters.

The average estimated RMS error for oblique photogrammetry was 1.4 m, eight times larger than the estimated 0.17 m RMS error of the 2 m DEMs used for ground control in the oblique surveys (Schilling et al., *in press*). It is not surprising that the RMS error for oblique DEMs is larger than the 2 m DEM, since error reported by oblique photogrammetry can be no smaller than the error involved in the 2 m DEM used to extract control points. Potential sources of this error discrepancy between techniques can be attributed to such things as sensor resolution, obliquity of images, software limitations, accuracy and precision of control points, and point determination (automated versus manual).

Average RMS residuals were utilized to evaluate the uncertainty associated with volume measurements. In order to make a direct comparison with vertical aerophotogrammetry, I adopted the same techniques as Schilling et al. (*in press*) for model uncertainty estimates. According to Schilling et al. (*in press*), volume uncertainty is a function of the average RMS residual error multiplied by the area of the growing dome. Area dimensions, for each model, were calculated in ArcMap using the 3D Analyst extension and the Area and Volume Statistics calculator. Area in m^2 for each model was input in an Excel spreadsheet and area values of the twelve DEMs were averaged to get an overall average of erupted area. Following the steps taken by Schilling et al. (*in press*), I multiplied the average area by the average RMS residual for all models, then divided that value by the average change in volume from model to model to produce an average volume uncertainty for the oblique DEMs.

For DEMs produced from oblique photographs taken between November 2004 and April 2007, RMS values of residuals averaged about 1.4 m in the x and y directions (planimetric coordinates) as well as the z direction (elevation coordinate). Multiplication of 1.4 m by the average area of the MSH crater surface affected by the extrusion of lava yields a volumetric uncertainty of 3.7×10^5 m^3, which is about 9% of the typical monthly extruded volume (4×10^6 m^3) inferred from differencing successive DEMs. This error estimate assumes a nearly worst-case scenario.

Overall, the level of uncertainty is relatively small when taking into account the type of survey conducted, the amount of material produced, and the obscurity of the basal subsurface topography from Crater Glacier. In relation to the estimated 4% volume uncertainty of the vertical aerophotogrammetric method (Schilling et al., *in press*), my

estimated 9% uncertainty is very promising in evaluating the success of using this method to accurately model dome growth.

3.2. Extrusion Rate Error

The error associated with the extrusion rate values derived from the estimated volumes for each DEM were calculated using Newton's Error Propagation Theorem (Stoer and Bulirsch, 2002):

$$\sigma_{rate} = \sqrt{\frac{1}{t^2}\left(\sigma_{vol}^2 + \frac{vol^2}{t^2}\sigma_t^2\right)}$$

Newton's theorem was chosen for the extrusion rate error calculation because the extrusion rates are based on two variables, time and volume. Newton's error propagation theorem calculates error for each rate based on four variables; t represents the time between successive photos (s), σ_{vol} represents the average volume error (estimated above), vol represents the volume change between successive dates, and σt represents the error in time associated with each date. The error or uncertainty of time is roughly twice the duration of a helicopter flight, if the time of day for each flight is known. The time of each set of photographs was unknown, but the date of acquisition gave an estimated error of 8 hours. This estimate takes into account variations of the time of day in which images were acquired. In other words, if one flight occurred early in the morning on a given date and the other occurred late on another date, then the uncertainty in the time interval between photos could be as much as 8 hours. Assuming the largest time uncertainty of 8 hours, the average extrusion rate uncertainty is 0.12 m^3/s.

33

4. RESULTS

Twelve DEMs were constructed from oblique overlapping aerial photographs to evaluate the growth of a lava dome inside the crater of Mount St. Helens during the period November 2004 to April 2007 (Fig. 12A-L). The majority of the DEMs are from the early stages (2004-2005) of the eruption when helicopter flights were deployed frequently. Additional oblique aerial photographs were taken by CVO scientists in the spring of 2006 and again in 2007 for continued documentation. Each DEM as well as the oblique photographs used to construct DEMs proved useful for qualitative evaluation of the morphology and growth of the lava dome. Observations and measurements described in this section were derived from the oblique photographs and their associated DEMs.

I follow the terminology of other workers regarding the evolving morphology and features in the crater of Mount St. Helens (Vallance et al., *in press*; Schilling et al., *in press*; Scott et al., *in press*): The dome growth that occurred from 1980 to 1986 produced several extrusions that formed a single lava dome, known as the *1980-1986 Dome*. Dome growth that began on October 11, 2004 has continued to present without repose. The dome growth is referred to as a single lava dome comprising several individual extrusions. The individual extrusions that began in October 2004 and continue to present are referred to as *spines* rather than lobes because of their solid-state character (Blake, 1990). When the spines are smooth and recumbent, implying that the vertical component of dimension is less than the horizontal component, they are referred to as a *whaleback*. The spines extruded at Mount St. Helens have different shapes that include fins (vertical faces of lava), whalebacks, and conical domes of blocky material, each having changed shape with time via internal and external deformation.

34

The oblique aerial photographs used in this study were first taken two months after the initial unrest at Mount St. Helens. Because of this delay, information about the beginning of the eruption is not contained in the photographs. To enable analysis from the start of the eruption, I augment the photogrammetry data with observations from other workers. September 23, 2004 marked the beginning of volcanic unrest at Mount St. Helens with intense seismic swarms (Moran et al., *in press*). From September 23 to October 10 there were several events of vent clearing and phreatic explosions (Shilling et al., *in press*). These events were accompanied by accelerated uplift of Crater Glacier. The first appearance of dacite lava occurred on October 11, 2004 with a fin shape of solid dacite lava (Spine 1), growing in a near-vertical fashion (Scott et al., *in press*). Between October 11 and October 15, Spine 1 grew and broke apart. October 15 – 24 marked the growth period of Spine 2. On October 25, recumbent Spine 3 began to emerge and grow toward the south crater wall (Shilling et al., *in press*).

4.1. Dome Growth: 2004 – 2007

Here I review the evolving morphology of the dome, as seen in the twelve sets of oblique aerial photographs and the resulting DEMs. Table 5 summarizes the character of eruption and activity of the volcano during this interval.

November 20, 2004 was the first day that overlapping oblique aerial photographs were taken of the growing dome inside the crater of Mount St. Helens. As stated above, by this date dome growth had already produced two spines of dacite, and a third was forming. Oblique photography and the DEM show that Spine 3 was in a recumbent growth phase, forming a low angle cylindrical-like smooth plug that broke through the

existing Crater Glacier surface (Fig. 13). The smooth appearance of the solid dacite of

Spine 3 inspired the term whaleback to describe its morphology (Spine 3 is also known as

Whaleback 1). Spine 3 formed just south of the stump of Spine 1 and was extruded

directly south of the 1980-1986 Dome. Spine 3 had a NW-SE orientation and by

November 20, 2004 had reached the south crater wall. The east portion of the new dome

was dominated by the presence of this whaleback; it had a center 155 m wide (as

measured from the DEM) and tapered at both the north and south ends (Figs. 12A, 13).

The west side of the dome began to spread out with a talus apron formed by the

disintegration of Spine 3 and remnants of Spine 2.

Table 5. Characteristics of lava dome growth from November 2004 – April 2007.

Date of oblique photography	Active spine	Dome length (long-axis in meters)	Dome width (long-axis in meters)	Character of eruptive activity (in bold)
11/20/2004	Spine 3	345	254	**Exogenous**
11/29/2004		511	352	Spines dominate dome growth
01/03/2005	Spine 4	464	387	Dome growth migrates east
02/01/2005		526	500	Talus fans to the north
02/22/2005		600	460	
03/11/2005		720	510	
04/10/2005		730	583	Spine begins to disintegrate
05/12/2005	Spine 5	680	535	
06/15/2005		627	630	Westward migration of growth
10/12/2005	Spine 6	870	600	**Endogenous**
05/30/2006	Spine 7	920	600	**Exogenous/endogenous**
04/20/2007		1032	650	**Endogenous**

On November 29, 2004 the exposed base of Spine 3 continued to push against the south crater wall, while the recumbent spine gained 100 meters in length (Fig 12B). The perimeter of extruded lava remained constant on the east side of the dome and continued to fan out on the west side, in part, due to a large section of the southwest tip of Spine 3 having broken apart from impact against the crater wall.

No oblique photographs were taken in December of 2004, but the January 3, 2005 photographs and the DEM showed that a new spine, Spine 4, had begun growing and over-thrusting Spines 2 and 3, eventually pushing Spine 2 to the west and Spine 3 to the east. During this time, spine and dome growth continued to the south and began migrating east as well. Talus aprons from the previous three spines began to fill the outskirts of the growing spine that dominated the growth of the dome (Figs. 12C, 14). Spine 4 was wider than the previous spines at 180 m in early January but had many similarities with Spine 3, which included a striated, gouge-covered surface, patterns of discoloration, and large cracks (Fig. 14 inset).

Over the period of one month, January 3 to February 2, 2005, the eruption added significant volume to the dome (Fig. 12D). Spine 4 (Whaleback 2) continued to grow south and east. The northern section of the dome consisted of the steep whaleback feature, while the south, east and west ends were covered by relatively steep talus slopes and remnants of previous spines. In early February, Spine 4 maintained a cylindrical like form that had a constant thickness of 150 m through the majority of its body and tapered to a steep slope at its southern extent, 325 m in length from the vent (Fig. 15).

Images of February 22, 2005 show the continued growth of Spine 4 (Fig. 12E). Sometime in mid-February, a significant portion of the west side of Spine 4 collapsed and

left a sizable scar in the smooth surface (Fig. 16). Spine 4 had gained 65 m in length since the beginning of February.

By March 11, 2005 dome morphology had changed very little from its form in late February (Fig. 12F). Spine 4 had gained an additional 60 m in length, totaling 450 m from vent to southern tip. Approximately 1/3 of the southwestern tip of Spine 4 had collapsed by this time adding significant talus to the west side of the dome.

April 10, 2005 images show the beginning of breakdown of Spine 4, with large rock fall scars on the east face and west side of the second whaleback (Fig. 12G). A series of northeast and northwest striking fractures, resulting from compression against the south crater wall, began to break apart Spine 4, leaving piles of talus and several large block remnants (Fig. 17) (Scott et al., *in press*). Fracturing throughout Spine 4 caused further westward migration of dome material. Spine 4 reached a maximum length of 480 m and width of 160 m.

Oblique aerial photographs and the DEM show the growth of Spine 5 on May 12, 2005 (Figs. 12H and 18). Spine 5 had a smooth appearance with large cracks and patches of discoloration from gases (as did the previous two spines), but it had a much steeper slope of 60-70 degrees on all sides. Spine 5 marked the beginning of westward migration of dome growth with its locus roughly 130 m west of previous spine growth. Breakdown of Spine 4 and new growth of Spine 5 created a trench between the two that filled with talus and rock debris from spine fragmentation, leaving the perimeter of rock debris nearly unchanged.

June 15, 2005 images show the continued growth of Spine 5, which was shorter, 132 m in length, and narrower, only 110 m at the base, than Spine 4 (Fig. 12I). Spine 5

maintained its steep slopes of 60 degrees in all directions. Through the remaining summer months of 2005 no oblique imagery was acquired.

The next dataset available from oblique aerial photogrammetry was in October 2005 (Fig. 12J). By this date Spine 5 had broken apart, leaving mega-block remnants and piles of talus. The locus of growth for Spine 6 lay more than 200 m west-northwest from that of Spine 5, significantly transferring dome growth to the west. A small portion of Spine 6 had the typical smooth surface with gouge of previous spines and was oriented southwest-northeast, but the majority of the spine had already broken apart to form a conical talus pile to the southwest of the 1980-1986 Dome. During this time, the majority of dome growth was endogenous (growing from within the talus, i.e. inflation). Talus filled the gaps left between spines and covered the perimeter of dome growth. Long-axis length of the dome was nearly 900 m with a long-axis width of 600 m (Fig. 19).

Seven months of the eruption elapsed until the subsequent deployment of another oblique photogrammetry flight on May 30, 2006. By this time Spine 7 had emerged ~170 m southeast of Spine 6 in the talus trench that formed when dome growth migrated west (Fig. 12K). Spine 7 had a near vertical face striking north-south that enveloped the east side of the conical talus dome that began growing mid-summer 2005. The growing dome had essentially filled the entire area of the crater floor south of the 1980-1986 Dome.

Nearly a year later, on April 20, 2007, the final set of oblique aerial photographs for this project were taken. Endogenous growth dominated eruptive activity during the last documented interval. The west section of the new dome lost over 60 m in elevation

but continued to grow in circumference to an average diameter of 500 m. Two and a half years of dome growth had formed a composite dome larger than the 1980-1986 Dome (Fig. 12L).

4.2. Quantitative Description of Dome Evolution

DEMs permit quantitative analysis of the evolving dome growth of Mount St. Helens. Quantitative measurements of significance to this study, which include dome height, eruptive volume, and extrusion rate through time, can be seen in Table 6. Dome height was measured from the highest point on each DEM to the point directly below it on the 1986 DEM surface. Fig. 20 shows a time-series of dome height and includes significant seismic, collapse, and deformation events. A closer examination of seismic event spacing, magnitude, and resultant daily seismic energy is provided in Fig. 21. Eruptive volume was calculated using an AML script in ArcInfo that subtracted each of the twelve DEMs derived from oblique photogrammetry from a 1986 DEM that is representative of the pre-eruption and pre-glacier crater floor. A full description of this technique can be found in the methods section (2.6). Estimates of the rate of newly extruded lava were made by differencing successive DEMs and dividing the volume difference by the amount of elapsed time (s) between sequential DEMs. Volume calculations and extrusion rates through time can be seen in Table 6 and Fig. 22.

Dome growth has continued without repose since the October, 2004. A rapid increase in dome volume through the first seven months of oblique photogrammetry surveys is seen in Fig. 22. From June 2005 to April 2007, the dome growth curve began to level out and has remained at a relatively constant growth rate of less than 1 m^3/s.

40

Both variables follow a similar curve from 2004 to 2007. A more descriptive evolution

of dome growth follows:

Table 6. Extruded lava volume, lava extrusion rate, and dome height (above 1986 crater floor) values of the 2004-2007 eruption of Mount St. Helens, with associated error estimations as determined by the method discussed herein.

Date of oblique photography	Total extruded lava (x 10^6 m^3) ± 4x10^6 m^3	Lava extrusion rate (m^3/s) ±.12 m^3/s	Dome height (m) ± 1.4 m
11/20/2004	15	4.3	263
11/29/2004	22	(8.5)	274
		5.1*	274
01/03/2005	26	1.3	304
02/01/2005	35	3.9	327
02/22/2005	38	1.3	325
03/11/2005	41	2.5	318
04/10/2005	47	2.2	323
05/12/2005	56	3.2	371
06/15/2005	60	1.4	363
10/12/2005	68	0.8	290
05/30/2006	85	0.9	375
04/20/2007	94	0.3	317

* Extrusion rate recalculated without using data from 11/20/2004 and used when graphing extrusion rate vs. time (Fig. 28). Both extrusion rate values are plotted in Fig. 22. Volume estimates for 11/20/2004 were determined to be underestimated, therefore adding error to the time-averaged extrusion rate of 11/29/2004.

The extrusion rate of November 20, 2004 was calculated assuming a start date of

October 11, 2004, because as this was the first date lava was extruded to the surface,

according to field observations (Vallance et al. *in press*). The first date that oblique

photography was conducted, November 20, 2004, yielded a dome volume of 15x10^6 m^3.

Persistent steaming at the vent obstructed views of the growing dome as seen in Fig. 13.

Steam obstructed nearly the entire west and north side of the dome, and the helicopter did

not fly to the southern end of the dome to capture images from that vantage point.

Because of this limited coverage, the DEM produced from the oblique photographs had limited sections where I could pick points located in pairs of photographs and thus the DEM is coarse and volume is likely underestimated. Nine days later on November 29, 2004 oblique photographs were able to capture the entire dome and the DEM volume estimate was $22\times10^6\,\mathrm{m}^3$, a significant increase from the previous DEM. The dome was extruding at a rate of 8.5 m^3/s, a rate that is overestimated based on the fact that the previous DEM volume was underestimated for reasons given above. By the end of November 2004 the new dome had reached 2295 m in altitude, 290 m above the 1986 crater floor surface.

The DEM produced from oblique photography taken January 3, 2005 established a total dome volume of $23\times10^6\,\mathrm{m}^3$ and an extrusion rate of 1.3 m^3/s between November and January. The highest point of the dome in early January reached 2304 m altitude, 304 m above the 1986 crater floor.

DEM calculations show the dome had grown an additional $10\times10^6\,\mathrm{m}^3$ a month later on than February 2, 2005, because of an accelerated extrusion rate of 3.9 m^3/s. The DEM produced from oblique photographs taken on February 22, 2005 the showed extrusion rate had declined by over 2.5 m^3/s to 1.3 m^3/s, but total erupted lava reached a volume of $38\times10^6\,\mathrm{m}^3$ and reached an altitude of 2342 m.

By March 11, 2005 extrusion rate had nearly doubled from the end of February, reaching a rate of 2.5 m^3/s and total dome volume reached $41\times10^6\,\mathrm{m}^3$. A short-lived explosive event occurred on March 8, 2005, causing the height of the dome to decrease slightly from 325 m in February to 318 m above the 1986 crater floor on March 11, 2005.

The extrusion rate remained relatively stable between March and April 2005 at 2.2 m^3/s. On April 10, 2005, seven months after the first report of lava having reached the surface, dome volume had reached $47x10^6$ m^3, half the volume of the 1980-1986 Dome.

The extrusion rate had once again increased from the previous month to 3.2 m^3/s, increasing dome volume to $56x10^6$ m^3 on May 12, 2005. Dome height had reached an apex of 371 m above the 1986 crater floor with new growth of Spine 5.

On June 15, 2005 total dome volume was $60x10^6$ m^3 and lava extrusion rate had decreased by over a half to 1.4 m^3/s. Dome height had decreased slightly with the break-up of Spine 5, the highest point on the dome was 2347 m in altitude and, at this location was 363 m above the 1986 crater floor surface.

The period of westward migration of the locus of growth and emergence of Spine 6 on October 10, 2005 had a slightly declined extrusion rate of 0.8 m^3/s. Total dome volume had reached $68x10^6$ m^3. Dome height was at its lowest point since early in the eruptive episode (November 29, 2004), at a height of 290 m above the crater floor.

Over the period of seven months extrusion rate had remained relatively constant at just under 1 m^3/s from the rate between October 10, 2005 and May 30, 2006. Dome volume was $85x10^6$ m^3. Dome height had once again reached the apex at 375 m, reaching the altitude of the lowest point on the crater rim (2363 m altitude) with the growth of Spine 7.

Almost a year later on April 20, 2007 extrusion rate had declined to 0.3 m^3/s. Dome volume totaled $94x10^6$, $2x10^6$ m^3 greater than the volume of 1980-1986 Dome.

Dome height had been reduced by 60 m with the break-down of Spine 7 and endogenous growth dominated the character of extrusion.

4.3. Comparison to Vertical aerophotogrammetry Technique (USGS DEMs)

Qualitative comparison between the technique employed in this study, oblique photogrammetry, and the vertical aerophotogrammetry technique used by the U.S. Geological Survey can be seen in Fig. 23, which shows a selected pair of DEMs from the same date constructed by means of each technique. A quantitative comparison can be achieved by looking at volume differences and estimation of uncertainty calculated for each technique.

According to Wolf and Dewitt (2000), the size of residuals is not always an ideal indicator of project accuracy or error; projects with small residuals may be inaccurate in terms of absolute position marking. Because of this unknown, Wolf and Dewitt (2000) advise the only way to disclose a systematic error (i.e. datum, map scales and projections) is to perform field tests or comparisons to surveys that have employed strong geodetic control. A comparison of this type is possible for this project since vertical aerophotogrammetric surveys were performed typically on the same day as oblique photogrammetry flights. Comparison of oblique photogrammetry employed in this study to vertical aerophotogrammetry techniques used by the USGS to construct DEMs is not only a good indicator of technique accuracy, assuming the USGS DEMs are close to 'truth', but also provides an evaluation of this technique in terms of volcano monitoring, cost effectiveness and future use.

Volume comparisons of dome growth between oblique and vertical

aerophotogrammetry techniques are shown in Table 7. Total dome volume estimates

measured by the two different techniques fall within each method's error, with the

exception of January 3, 2005 (Fig. 24). I calculated volumes using the same method

(described in section 3.2) for both oblique and vertical aerophotogrammetric derived

DEMs.

Table 7. Volume comparisons between vertical aerophotogrammetry and oblique
photogrammetry techniques.

Date of oblique photography	Oblique Volume (x 10^6 m^3)	USGS Volume (x 10^6 m^3)	% Comparison	*Adjusted USGS Volume (x 10^6 m^3)	% Comparison
11/20/2004	15	No data	------	†15	98
11/29/2004	22	21	101	21	96
01/03/2005	26	31	84	24	96
02/01/2005	35	35	100	34	97
02/22/2005	38	39	96	39	105
03/11/2005	41	42	98	41	99
04/10/2005	47	No data	------	No data	------
05/12/2005	56	No data	------	No data	------
06/15/2005	60	54	111	57	96
10/12/2005	68	No data	------	†67	99
05/30/2006	85	82	104	79	94
04/20/2007	94	93	101	No data	------

* USGS DEM volume calculated using extruded lava boundary determined from the
oblique photographs.
† Indicates dates that do not directly correspond. Closest dates were used for
calculations.

On average, volume calculations from the oblique photogrammetry DEMs came within

5% of volume calculations from vertical aerophotogrammetry DEMs. Volume and

percent differences for each date in which both techniques were employed at Mount St.

Helens can be seen in Fig. 25A. This method yields the best comparison between the two

techniques because interpretation and mapping of extruded lava boundaries may differ between users.

To provide a comparison of volume estimates between techniques using a single variable, volumes of both sets of DEMs (oblique and vertical aerophotogrammetric) were calculated using the same extruded lava boundary. The volume and percent discrepancy of the DEMs using the same clipping boundary are shown in Fig. 25B. This volume calculation method yields an average 2% volume discrepancy between techniques. This comparison tests only the DEM difference, not the additional difference of interpretation of extruded rock boundaries.

5. DISCUSSION

5.1. Dome Growth

The chronology of dome growth between 2004 and 2007 at Mount St. Helens reveals a number of trends including: (1) a transition from purely exogenous to predominately endogenous growth; (2) migration of the locus of dome growth: first in an eastward direction, and then westward; and (3) an overall decline in extrusion rate through time. These trends can be explained by investigating variables involved in the dome growth at Mount St. Helens.

5.1.2 Dome Growth Mechanics

Characteristics of the 2004-2007 dome growth (dome height, dome volume, extrusion rates, and migration of flow) calculated during this study are used to qualitatively explore the sub-surface mechanics driving the on-going eruption of Mount St. Helens. A goal of this study is to examine dome growth mechanics expressed in dome height and extrusion rate variations through time. Extrusion rates and volume estimates spanning two and a half years of eruptive activity at Mount St. Helens provide a framework to answer some fundamental questions about dome growth. I pose two hypotheses: First, as gravitational load (expressed as height) on an active dome increases, dome stability will decrease. Second, as the mean output rate varies over different periods of time, these variations will change the character of eruptive activity.

Laboratory, field and theoretical studies have been conducted by Melnik and Sparks (1999) and Fink and Bridges (1995) that examine the relationship between dome

47

height and extrusion rate. Melnik and Sparks (1999) studied the October 1997 eruptive period at Soufriere Hills volcano and found an inverse relationship between these two variables: extrusion rate declines as dome height increases (Fig. 26). This observed relationship at Soufriere Hills volcano did not correspond to their analytical model that predicted an oscillating pattern expressed by the two variables if the eruption is in steady-state (Fig. 26), which was addressed via the argument that at low extrusion rates and large dome heights the eruption cannot be in steady state. For steady-state eruptions, Melnik and Sparks (1999) predict dome height directly from extrusion rate. The extrusion rate is thought to be strongly related to magma overpressure in the chamber below.

Fink and Bridges (1995) examined several groups of natural lava domes including Mount St. Helens (1980-1986 Dome) and Soufriere Hills, and they also conducted scaled laboratory experiments to simulate dome growth. Their study found that dome height increased steadily with erupted volume, and the rate at which height increased with volume depended linearly on the time-averaged effusion rate. According to Fink and Bridges (1995), the accumulation of lava above the vent acts to increase the vent pressure and reduce the eruption rate. In turn, the eruption rate determines how the eruption volume changes with time.

Reducing these models to factors observable with photogrammetry, Melnik and Sparks (1999) argue that dome height is controlled by extrusion rate; Fink and Bridges (1995) argue that dome height is limited by gravitational load. One way to reconcile the two models could be an alternating system between gravitational-load- and extrusion-rate-controlled dome heights. To investigate this possibility, I examine data derived from

oblique photogrammetry (presented in Section 4), augmented with records of seismicity

and vertical aerophotogrammetry (Moran et al., *in press;* Schilling et al., *in press*).

A weak inverse correlation exists between dome height and extrusion rates from

this study (Fig. 27). The correlation is understandably low, because the relationship

includes only two variables of dome growth, suggestive of an unrealistically simple

process. Although this presentation shows that, on average, dome height has decreased

with increasing extrusion rate during this eruption, closer examination of the time-series

(Figs. 20 and 28 discussed below) shows that there are periods when the two are

positively correlated. Comparison of these two variables with additional observations

including spine growth and disintegration, seismicity, and locus of growth migration

provide a more thorough picture of the relationship between dome height and extrusion

rate. Fig. 20 illustrates a more complete chronology of the 2004-2007 dome-building

eruption of Mount St. Helens, with dome height variations through time and significant

seismic, deformation, and explosive events. To investigate trends found from the data

collected in this study it is necessary to also include data collected by the U.S. Geological

survey from vertical aerophotogrammetric surveys to confirm trends since the vertical

aerophotogrammetric DEMs are acknowledged to be more accurate in most cases. This

unique combination of datasets also provides a more substantiated argument for trends

found in the dome growth variables.

Examination of variables involved in dome growth at Mount St. Helens (Figs. 20,

24, and 28) suggests a correlation between dome height and such things as spine

fragmentation and collapse, spine growth and seismicity levels. These correlations are

described below:

Extrusion rate variations and total dome volume can be seen in Fig. 22. Dome height, as measured from the 1986 crater floor to the apex of the growing dome, expresses an oscillatory behavior from November 2004 to April 2007. Between November 2004 and January 2005 dome height increased as extrusion rate decreased (Fig. 28). During February 2005, both dome height and extrusion rate increased according to measurements by both photogrammetric techniques. The positive relationship between dome height and extrusion rate during this phase may be attributed to the growth of a new spine as well as a significant explosive event that occurred in mid January. The photographic data are not sufficient to negate or confirm the reason for this positive relationship. From February 1 to 22, 2005 dome height and seismicity remained relatively stable as extrusion rate declined significantly. Spine 4 dominated the area of dome growth and, according to the dome height plots (Fig. 20) had reached the apex of its growth. Portions of Spine 4 began to collapse sometime in February, but it seems that the solid plug-like morphology of this spine added significant pressure to the vent, causing a dramatic decrease in extrusion rate.

Extrusion rates and dome heights from late February 2005 to April show a strong inverse relationship. From April 2005 to May 2005 extrusion rate increased along with dome height. This increase in extrusion rate and dome height cannot be validated by vertical aerophotogrammetry because no DEM from May 2005 was made by this method. If the relationship found in the oblique dataset is true, a possible explanation is as follows: In April, Spine 4 encountered the south crater wall and began to disintegrate, while Spine 5 emerged in an eastward migration of the locus of growth. This continued

migration and new spine growth may account for the increase in dome extrusion rates and dome height at this time.

Oblique photography was not captured between June 15, 2005 and October 10, 2005. Vertical aerophotogrammetric data show that extrusion rate increased as dome height decreased from July 2005 to August 2005, and from August to October 2005 the variables exhibit a positive correlation, as is seen by oblique photogrammetric data. In May, dome height reached an apex of 375 m above the 1986 crater floor. After reaching this height, Spine 5 began to break apart in significant dome collapse events. Seismicity also declined substantially in event size and rate at this time (Moran et al., *in press*). From this data, I surmise that overpressure of the growing dome on the vent slowed dome growth (extrusion rate) significantly at this time.

Both oblique and vertical aerophotogrammetry data show that from October 2005 to April 2007 extrusion rate and levels of seismicity remained relatively stable, while dome height began to increase. In addition, October marked the beginning of westward migration of the locus of dome growth and a transition from purely exogenous dome growth to a combination of predominantly endogenous dome growth and lesser amounts of exogenous spine growth.

These observations suggest that dome height and extrusion rate play a significant role in the character of eruptive activity. During times of exogenous dome growth, the feedback between dome height and extrusion rate is apparent: Dome height directly influences the decline of extrusion rate by gravitational overpressure on the conduit. During periods of exogenous growth the solid spines are clearly connected to the vent, imposing a direct load onto the area of lava extrusion. The solid nature of exogenous

growth at Mount St. Helens also favors spine destabilization, which ultimately leads to spine collapse or migration of the vent, and renewed increase in extrusion rates. During times of endogenous growth the relationship breaks down: dome height increases steadily to a maximum point, then declines, but extrusion rate remains relatively stable. One possible explanation of this correlation is that during periods of endogenous growth, material accumulates over a larger area, not just directly over the conduit, and thus the feedback is not as apparent or strong.

Another aspect of this relationship suggests a possible threshold at which a growing dome becomes inherently unstable due to perturbations such as unloading of the pressurized conduit by dome collapse. Close examination of this relationship provides preliminary evidence of a critical threshold at which dome height reaches an apex, possibly resulting in the migration of the point of extrusion or a slowing and possible cessation of the eruption. Dates that suggest this relationship are May 12, 2005 and May 30, 2006 when dome heights reached maximum values of ~370 m. On May 12, 2005 this maximum dome height was followed by a significant westward migration in the locus of dome growth as well as a change from exogenous to endogenous eruptive character (Fig. 20). Data following May 30, 2006 are limited but show the maximum dome height ~370 m attained during exogenous growth, followed by a decline in dome height during endogenous growth and continued westward migration.

This study examined a much broader timescale than that studied by Melnik and Sparks (1999), and a single episode of dome growth, unlike Fink and Bridges (1995). The temporal resolution of this study is limited and thus it would be difficult to produce a

52

more robust relationship between dome height and extrusion. If oblique photography

flights continue, a more comprehensive look at this relationship could be accomplished.

A more robust dataset (in terms of improved temporal resolution) needs to be acquired

and factors such as overpressure of the conduit due to gravitational load and its effect on

the rate of dome growth should be considered further, in order to evaluate the sub-surface

processes affecting Mount St. Helen's volcanic system. Additionally, further oblique

photogrammetry surveys at Mount St. Helens are warranted to better constrain models

related to dome growth rates, specifically the relationship between dome height and

extrusion rate, with much higher temporal resolution than is currently employed.

5.2. Methods

The nature of this project, which consisted of using a new technique in

photogrammetry to collect and analyze spatial data of the growing dome of Mount St.

Helens volcano, is inherently complex. As with all scientific experiments, experience has

shown which portions of this project worked successfully and which can be improved

upon for future studies. Analyses of the selected study site, instrumentation and software,

field and processing methods, and comparison between photogrammetric techniques are

described in this section.

5.2.1. Study Site: Mount St. Helens

It should be addressed that the methods of this study were not pre-planned before

the onset of eruptive activity in September of 2004. Oblique photographs were acquired

to use with specific software not utilized by this study. All datasets used in this study

were acquired before software was chosen or a course of action, with respect to dataset analyses, was planned. The study site, software, and hardware used in this study have been combined to provide a successful evaluation of a method and of dome evolution at Mount St. Helens volcano.

The selection of Mount St. Helens as the target volcano for this study was significant to the success of this project. Mount St. Helens' proximity to roads and cities makes it an easily accessible volcano. In addition, it is roughly 50 km from the USGS Cascades Volcano Observatory office, making travel to the volcano by helicopter and car, unproblematic. The volcano's renewed activity in September 2004 made it a perfect study site to experiment with new techniques to monitor and study dome growth. Another advantage is the robust monitoring structure established at the volcano, which includes a dense network of permanent and campaign GPS stations, seismometers, permanent terrestrial camera stations, tiltmeters and routine gas sampling, vertical aerophotogrammetric surveys, and petrologic analyses. These datasets allow comparison between variables of dome growth for a better understanding of volcanic processes occurring at Mount St. Helens. Field crews from the USGS regularly take helicopter flights to the volcano for monitoring. Because of this frequency, I and other workers were able to take a camera on flights and capture oblique photogrammetry for this project by helicopter. Considering the nature of the available equipment and the financial limitations of this project, Mount St. Helens was the ideal volcano to support this study. The same conveniences might not be available at other volcanoes of interest, particularly in remote locations, which could limit the applicability of the method.

5.2.2. Instrumentation and Software

The Nikon D70 digital SLR camera used for image acquisition proved efficient and affordable use in this project. The D70 has since been replaced by the similar D80, but a D70 body with an 18-70 mm Nikkor lens can be purchased for less than $1,000. Any off-the-shelf digital camera could have been used for this project but the Nikon D70 offers features such as interchangeable lens capability, infinity focus setting, RAW format options, auto and manual focus. The camera is user friendly and images can be easily and rapidly downloaded in the field or office, all of which make the Nikon D70 a leading choice in instrumentation used for this method.

Arguably the most significant portion of this research project in terms of project objectives is the processing software for oblique imagery. PhotoModeler was the choice of software for this project because it met two criteria: (1) it must be able to process oblique digital images with limited ground control and still reach a certain level of accuracy, and (2) be relatively inexpensive (less than $1,000) and easily accessible. Alternative software packages were tested for use in this project but required that camera locations be known at the time of image acquisition. The photographs for this project were acquired before the development of this project, and thus locations were not recorded, requiring an adaptable software program such as PhotoModeler. The built-in camera calibration extension of PhotoModeler is the most advantageous feature of the software. This extension allowed the use of a commercial grade, non-metric camera to be used as the sensor for image acquisition in this project, which is a significant feature that allows the method employed in this project to be cost-effective. In addition, the software is consumer-grade and inexpensive (~ $800), a small price relative to the cost of other

photogrammetric software package ($5,000 to $70,000). Additionally, some photogrammetric software packages require specific hardware to run the programs, which can cost up to $500,000 and require rigorous training to operate, adding to the total cost. Additionally, in order to demonstrate the potential and field-worthy nature of this novel technique, the software must be able to accurately generate DEMs, which are then used to quantify the volume of the dome. Results from processing twelve sets of oblique photographs with PhotoModeler software support that this software, when incorporated with the instrumentation used in this project, is low-cost, time-efficient, simple, and accurate.

5.2.3. Processing Time

Once methodology had been established for this project, a single DEM derived from a set of oblique photos could be produced in about 4 hours. This processing speed puts oblique photogrammetry far above traditional vertical aerophotogrammetry in turn-around rate, which typically takes two to three weeks from flight to DEM. A significant goal of this study is reached in producing a technique for fast hazard evaluation in the event that volume analysis is required at an active volcano.

5.2.4. Comparison of Techniques

As stated in the results section of this manuscript, on average DEMs from oblique photogrammetry and vertical aerophotogrammetry had volume calculations within 5% of each other. Significant variation (>10%) of dome volumes for January 3, 2005 and June

15, 2005 can be attributed to adverse atmospheric effects and insufficient photographic coverage.

On November 20, 2004 persistent steaming at the vent during image acquisition limited visibility of the spine and extent of extruded lava, thus the precision of the DEM from oblique photography is reduced. Because of this obstruction of view, volume calculations and extrusion rate for November 20, 2004 are below expected values (15×10^6 m^3). Nine days later another set of oblique aerial images were captured. At this date, there was little to no steaming and images were able to capture the entire dome and emerging spine, resulting in volume measurements significantly greater (and probably more accurate, in my opinion) than those from nine days previous and more representative of the volume of the dome.

Oblique images captured on June 15, 2005 were better able to capture the entire extent of dome growth than vertical aerial photographs used for vertical aerophotogrammetry due to persistent steaming at the vent (Fig. 23). The obliquity of view allowed for a complete view of the north side of Spine 6 and thus the volume calculation for this date made by oblique photogrammetry is significantly greater than volume calculated by vertical aerophotogrammetry, and likely more accurate.

5.2.5. Point Density Test

DEMs from oblique photography were constructed by adding as many reference points as could be identified in a group of photographs. This selection process resulted in varying numbers of points which make up each oblique photogrammetric DEM (Table 3). A significant question that arises from this method is how many points are sufficient

to make a DEM that achieves a given accuracy, with respect to the maximum point DEM

from oblique photography and the high point density DEM made by vertical

aerophotogrammetry? To assess this, I selected a relatively detailed DEM (oblique) for

which there was a corresponding vertical aerophotogrammetric DEM. The June 15, 2005

DEM was selected based on its relatively high point total (~800) and the fact that it

agrees with the vertical aerophotogrammetric DEM to within 4% when the same extruded

rock perimeter is used. To test the idea of a threshold, at which the number of points

deviates significantly from either DEMs (oblique or vertical aerophotogrammetric). I

used a random number generator in Microsoft Excel to select arbitrary subsets of points

(650, 450, 250, 150, 100). Five subsets of each point total were generated, and a DEM

was constructed from each, twenty-five in total, all having the same extruded lava

perimeter (made from 50 perimeter points) used for the original June 15, 2005 oblique

DEM. Volumes were calculated with the AML script used to calculate original volumes

for each epoch and the 1986 DEM used as a baseline. Discrepancy in volume versus

number of points (Fig. 29A) show that as the number of points in the model decreases,

the deviation from the expected volume increases. The volume of the ~800 point oblique

DEM and the point subsets of 250, 450, and 650 all fall within the error of the oblique

DEM (in either the positive or negative). The volume from the vertical

aerophotogrammetric DEM is smaller than all subset models (including the 800-point

DEM). The volume discrepancy between oblique subsets and the vertical

aerophotogrammetric DEM may be attributed to difference in coverage of the 2004-2007

dome on the date of June 15, 2005 (see section 5.2.4). Therefore I use the 800-point

volume (rather than the USGS vertical aerophotogrammetric volume) as my reference

value for assessing precision of the subset models. A plot of percent agreement between the 800-point oblique DEM and the point subsets illustrates that percent agreements deviate as point numbers decrease (Fig. 29B.). This is also shown in Fig. 30, which plots standard deviation represented of each point subset (650, 450, 250, 150, 100).

All point subset volume calculations agree relatively well with the volume of the 800-point oblique DEM. This agreement is the result of using a constant perimeter for each volume calculation. As described in section 2.6, the perimeter of extruded rock is projected vertically downward to the 1986 baseline DEM when calculating volume. The cylinder-like shape of the volume below the glacier has a strong influence on volume estimations. To confirm the significant role that the extruded lava perimeter plays in volume estimation, I re-calculated the twenty-five DEMs using a flat plane (from the lowest point on the perimeter) as a surface and again found that each subset of points agree relatively well with the 800-point oblique DEM. Using the 800-point DEM, which had a perimeter made of fifty points, I also calculated volume by subtracting 10 perimeter points sequentially until no perimeter existed. As a result of a variable perimeter, volume calculations, keeping the same flat plane used for other calculations, deviate, on average, 3.5% from the volume of the 800-point DEM. This result suggests that an accurate perimeter is important for a good volume calculation.

Qualitatively, the more points, the more detailed the DEM, and the more closely it may represent the actual morphology of the surface. The tests suggest that an inclusive perimeter is key in volume estimations, this is especially true if the baseline DEM is lower in elevation than the points which make up the perimeter, as is the case in this study. For rapid assessment of volumes and extrusion rates, relatively few points are

required: a good perimeter and as few as one (highest elevation) point in the interior and a minimum point density can be suggested to users. This of course, depends on the complexity of the terrain being modeled. For a closer representation of the form of the dome, it is suggested that a dense (i.e. as many points as can be located given the resolution of the image) be added to the model. DEMs in this study that have 400 or more points better represent the form of the dome than those models with lower point densities. With 400 points as a threshold to produce an agreeable DEM, point density of a minimum of 1 point per 800 m^2 can be suggested (Table 8).

Table 8. Point density calculations for June 15, 2005 DEMs based on point subsets within a constant area of 322540 m^2. The area is defined by the 50 point perimeter used for volume calculations.

Number of Points	Point Density (1 point per m^2)
800	403
600	538
400	806
200	1613
100	3225
50	6451

5.2.6. Recommendations

A point that should be addressed is that this study has presented a special case with respect to the fact that DEMs from vertical aerophotogrammetry were already established to use for control and comparison, and that the U.S. Geological Survey, Cascades Volcano Observatory made a considerable investment in helicopter flights during the eruption. It cannot be anticipated that the same resources will be available at other volcanoes during eruptions. In the more likely case that DEMs are not already

available and helicopter support is at a premium, I offer the following recommendations to provide flexibility of this method in application to other volcanoes:

Ground control used for this method can be acquired from several different methods. If funding is sufficient, the optimum choice for ground control is to use a network of GPS (campaign or permanent stations). This method provides the most accurate and precise way of determining control for models, but can also be expensive with respect to the cost of GPS and the deployment of the stations around the volcano, which may require helicopter assistance. The simplest is the use of topographic maps, though this technique involves error directly related to the contour interval of the map. Control can also be achieved by conventional trilateration from a theodolite, which does not require the use of a helicopter if the area surrounding the volcano is accessible by vehicle or hiking. One way to avoid using ground control is to capture the location (in x, y, z) of the camera at the time of image acquisition. This can be possible by using a kinematic GPS in the helicopter or near the camera (if images are taken from the ground) or utilizing a GPS hot shoe attachment, available on some new digital cameras. Any of the above methods will provide control for a model.

The use of a helicopter for image acquisition has played an important role in this thesis. Any type of aircraft provides a vantage point to easily capture a large area of dome growth by camera. In the case where helicopter support is unavailable, images could be acquired on the ground if vantage points were accessible. The optimum convergence angle for oblique photogrammetry is roughly 45°, but if angles greater than or less than the optimum are the only option, PhotoModeler is able to adapt to these variances of convergence.

In terms of the instrumentation used for image acquisition, the higher the sensor resolution the better. The Nikon D70 proved very successful for this project, but if newer models with higher resolutions are available, they provide an advantage. It is recommended that the lens used for image acquisition be fixed or that the operator of the sensor takes notes on different focal settings used, so that camera calibration can be as quantitative as possible.

The fact that this method is capable of using any off-the-shelf digital camera and images taken from the ground or from the air (whether vertical or oblique) to produce DEMs that agree well with DEMs produced by vertical aerial photography has an advantage in any situation of volcanic activity. The method has proved adaptable to limitations posed by ground control and photographic coverage.

More tests need to be conducted and refinements made in order for the accuracy of this method to be improved to levels of traditional photogrammetric surveys, but as the method stands, it proves useful as a source of supplemental and/or rapid and coarse data of dome growth measurements.

6. CONCLUSION

This research project was successful in applying a new technique to quantitatively measure dome growth at Mount St. Helens. The technique used oblique aerial photographs to create successive DEMs for qualitative and quantitative descriptions of the 2004-2007 eruption. The DEMs were used to calculate height, volume, and extrusion rate, and to track changes in these quantities through time. These quantities show a decreasing extrusion rate through time that has remained lower than 1 m^3/s since October 2005. Total dome volume as of April 2007 had reached 94×10^6 m^3, a larger volume than that of the 1980-1986 Dome. The quantitative evaluation of the DEMs tentatively suggest a possible relationship between dome height and extrusion rate, which varies with exogenous or endogenous growth of the dome.

Comparisons of traditional photogrammetry with oblique photogrammetry measurements show that volumes of volcanic dome growth measurements are reliable. Considering ever-increasing improvements in camera technology, commercially available software solutions, and computer processing speeds, oblique photogrammetry shows promise as an important new tool for volcano monitoring. Using inexpensive commercial photogrammetric software, a laptop PC, and sets of digital images taken from a standard digital camera, I was able to build DEMs, and to measure accurately the volume and average extrusion rate of an actively growing dacite dome in the crater of Mount St. Helens volcano. While there are many reliable methods of extracting growth data from active volcanoes, these methods are time consuming or costly compared to this technique. This study indicates that such a system can yield measured results from the images that are within an acceptable range of error. This method allows rapid and simple

surveys, producing results that are sufficiently accurate for the efficient monitoring and study of volcanic edifices. The method also shows promise for surveying areas that are not easily accessible and processing the data in the field or at temporary office locations with a laptop PC, desirable when fast hazard-mitigation is needed.

REFERENCES

Achilli, V., Baldi, P., Baratin, L., Bonini, C., Ercolani, E., Gandolfi, S., Anzidei, M., Riguzzi, F., 1997, Digital photogrammetric survey on the island of Vulcano, *Acta Vulcanolgica.*, v. 9, 1-5.

American Society of Photogrammetry and Remote Sensing, 2006, URL: http://www.asprs.org, accessed May 15, 2006.

Baldi, P., Bonvalot, S., Briole P., Coltelli, M., Gwinner, K., Marsella, M., G. Puglisi, G., Rémy, D., 2002, Validation and comparison of different techniques for the derivation of digital elevation models and volcanic monitoring (Vulcano Island, Italy), *International Journal of Remote Sensing*, v. 23, p. 4783-4800.

Baldi, P., Banvalot, S., Briole, P., Marsella, M., 2000, Digital photogrammetry and kinematic GPS applied to the monitoring of Vulcano Island, Aeolian Arc, Italy, *Geophysics Journal International*, v. 142, p. 801-811.

Barmin, A., Melnik, O., Sparks, R. S. J., 2002, Periodic behavior in lava dome eruptions, *Earth and Planetary Science Letters*, v. 199, p. 173-184.

Blake, S., 1990, Viscoplastic models of lava domes, In Fink, J. H., ed., Lava flows and domes, emplacement mechanisms and hazard implications: Berlin, Springer Verlag, *International Association of Volcanology and Chemistry of the Earth's Interior, Proceedings in Volcanology* 2, p. 89-126.

Bluth, G. J. S. and Rose, W. I., 2004, Observations of eruptive activity at Santiaguito volcano, Guatemala, *Journal of Volcanology and Geothermal Research*, v.136, p. 297-302.

Cecchi E., van Wyk de Vries B., Lavest J. M., Harris A., Davies M., 2003, N-view reconstruction: a new method for morphological modelling and deformation measurement in volcanology, *Journal of Volcanology and Geothermal Research*, v. 123, no. 1, p. 181-201.

Chandler, J., 1999, Effective application of automated digital photogrammetry for geomorphological research, *Earth Surface Processes and Landforms*, v. 24, p. 51 63.

Chandler, J. H. and Moore R., 1989, Analytical photogrammetry: a method for monitoring slope instability, *Quarterly Journal of Engineering Geology & Hydrogeology*, v. 22, no. 2, p. 97-110.

Clynne, M. A., Ramsey, D. W., Wolfe, E. W., 2005, Pre-1980 eruptive history of Mount St. Helens, Washington: *U.S. Geological Survey Fact Sheet 2005-3045*, 4 p., http://pubs.usgs.gov/fs/2005/3045.

Coulson, S. N., 1996, SAR interferometry with ERS, *Earth Space Review*, v. 5, no. 1, p. 9-16.

Crandell, D. R., Mullineaux, D. R., Rubin, M., 1975, Mount St. Helens Volcano: Recent and Future Behavior, *Science*, v. 187, no. 4175, p. 438-441.

Department of Ecology, *Geographical Information System Data*, October 9, 2006, <http://www.ecy.wa.gov/services/gis/data/data.htm>.

Doneus, M., 2001, Precision mapping and interpretation of oblique aerial photographs, *Archaeological Prospection*, v. 8, issue 1, p. 13-27.

Dzurisin, D., 2000, Volcano geodesy: challenges and opportunities for the 21st century, *Philosophical Transactions of the Royal Society A: Mathematical, Physical and Engineering Sciences*, v. 358, p. 1547-1566.

Dzurisin, D. 2006. Volcano deformation - geodetic monitoring techniques, *Springer Praxis Books in Geophysical Sciences*, Berlin, p. 439.

Dzurisin, D., Lisowski, M., Wicks, C., Poland, M., Endo, E., 2006, Geodetic observations and modeling of magmatic inflation at the Three Sisters volcanic center, central Oregon Cascade Range, USA, *Journal of Volcanology and Geothermal Research*,v. 150, p. 35-54.

Dzurisin, D., Lisowski, M., Schilling, S.P., LaHusen, R.G., Sherrod, D.R., Iwatsubo, E.Y., Diefenbach, A., Thompson, S.K., 2005, "Ground deformation associated with the 2004-2005 dome-building eruption of Mount St. Helens, Washington [abs.]", *American Geophysical Conference Fall Meeting 2005*, San Francisco.

Dzurisin, D., Wicks, C., Thatcher, W., 1999, Renewed uplift at the Yellowstone Caldera measured by leveling surveys and satellite radar interferometry, *Bulletin of Volcanology*, v. 61, no. 6, p. 349-355.

PhotoModeler, 2005, Eos Systems, Inc., (Version 5, Pro.)

Fink, J. H. and Bridges, N. T., 1995, Effects of eruption history and cooling rate on lava dome growth, *Bulletin of Volcanology*, v. 57, no. 4, p. 229-239.

Harris, A. J., Rose, W., Flynn, L, 2003, Temporal trends in lava dome extrusion at Santiaguito 1922-2000, *Bulletin of Volcanology*, v. 65, p. 77-89.

Harris, A. J. L., Murray, J. B., Aries, S.E., Davies, M. A., Flynn, L.P., Wooster, M. J., Wright, R., Rothery, D. A., 2000, Effusion rate trends at Etna and Krafla and their implications for eruptive mechanisms, *Journal of Volcanology and Geothermal Research*, v. 102, p. 237-270.

Heinz, G., 2002, Combination of photogrammetry and easy-to-use non-metric methods for the documentation of archaeological excavations, *International Archives of Photogrammetry Remote Sensing and Spatial Information Sciences*, v. 34, part 5, p. 379-383.

Herd, R. A., Edmonds, M., Venus, B. A., 2005, Catastrophic lava dome failure at Soufriere Hills Volcano, Montserrat, 12-13 July 2003, *Journal of Volcanology and Geothermal Research*, v. 148, p. 234-252.

Holcomb, R. T., Colony, W. E., 1995, Maps showing growth of the lava dome at Mount St. Helens, Washington, 1980-1986, *U.S. Geological Survey Map I-2359*, 1:5000 scale, 1 sheet with text.

Honda, K. and Nagai, M., 2002, Real-time volcano activity mapping using ground-based digital imagery, *ISPRS Journal of Photogrammetry and Remote Sensing*, v. 57, p. 159-168.

Hooper, D. M., Mattioli, G. S., 2001, Kinematic Modeling of Pyroclastic Flows Produced by Gravitational Dome Collapse at Soufriere Hills Volcano, Montserrat, *Natural Hazards*, v. 23, p. 65-86.

James, M. R., Robson, S., Pinkerton, H., Ball, M., 2006, Oblique photogrammetry with visible and thermal images of active lava flows, *Bulletin of Volcanology*, v. 69, p. 105-108.

Jordan, R., Kieffer, H. H., 1981, Topographic changes at Mount St. Helens: large-scale photogrammetry and digital terrain models. *In: Lipman, P., Mullineaux, D. (Eds.), The 1980 Eruptions of Mount St. Helens, U.S. Geological Survey Professional Paper*, v. 1250, p. 3-15.

Kaab, A., Funk, A., 1999, Modelling mass balance using photogrammetric and geophysical data: a pilot study at Griesgletscher, Swiss Alps. J. *Glaciolology*, v. 45, p. 575-583.

Kaneko, T., Wooster, M., Nakada, S., 2002, Exogenous and endogenous growth of the Unzen lava dome examined by satellite infrared image analysis, *Journal of Volcanology and Geothermal Research*, v. 116, p. 151-160.

Kerle, N., 2002, Volume estimation of the 1998 flank collapse at Casita volcano, Nicaragua - a comparison of photogrammetric and conventional techniques, *Earth Surface Process and Landforms*, v. 27, p. 759-771.

Lane, S. N., James, T. D., Crowell, M. D., 2000, Application of Digital Photogrammetry to Complex Topography for Geomorphological Research, *The Photogrammetric Record*, v. 16, p. 793-821.

Lu, Z., Wicks, C., Dzurisin, D., Power, A., Moran, S., Thatcher, W., 2002, Magmatic inflation at a dormant stratovolcano: 1996–1998 activity at Mount Peulik volcano, Alaska, revealed by satellite radar interferometry, *Journal of Geophysical Research*, v. 107 (B7).

Lynnerup, N., Vedel, J., 2005, Person identification by gait analysis and photogrammetry, *Journal of Forensic Sciences*, v. 50, issue 1, 7 p.

Major, J. J., Kingsbury, C. G., Poland, M. P., LaHusen, R. G. *in press*, Extrusion rate of the Mount St. Helens lava dome estimated from terrestrial imagery: November 2004 – December 2005, *In Sherrod, D. R., Scott, W. E., and Stauffer, P. H., eds., A volcano rekindled: the renewed eruption of Mount St. Helens, 2004-2006*: U. S. Geological Survey Professional Paper.

Melnik, O. and Sparks, R. S. J., 1999, Nonlinear dynamics of lava dome extrusion, *Nature*, v. 402, p. 37-41.

Mills, H. H., 1992, Post-eruption erosion and deposition in the 1980 crater of Mount St. Helens, Washington, determined from digital maps, *Earth Surface Processes and Landforms*, v. 17, p. 739-754.

Mikhail, E. M., Bethel, J. S., McGlone, J. C., 2001, Introduction to modern photogrammetry, *John Wiley & Sons*, New York, NY, USA. 2001. 479 p.

Miranda, P. J., Granados, H. D., 2003, Fast hazard evaluation employing digital photogrammetry: Popocatepetl glaciers, Mexico, Geofisica Internacional, v. 42, p. 257-283.

Moore, J. G., Lipman, P. W., Swanson, D.A., Alpha, T. R., 1981, Growth of Lava Domes in the Crater, June 1980 - January 1981. *In: Lipman, P., Mullineaux, D. (Eds.), The 1980 Eruptions of Mount St. Helens, U.S. Geological Survey Professional Paper*, v. 1250, p. 541-547.

Moore, J. G., Albee, W. C., 1981, Topographic and structural changes, March-July, 1980 – photogrammetric data. *In: Lipman, P., Mullineaux, D. (Eds.), The 1980 Eruptions of Mount St. Helens, U.S. Geological Survey Professional Paper*, v. 1250, p. 123-134.

Moran, S. C., 1994, Seismicity at Mount St. Helens, 1987–1992: Evidence for repressurization of an active magmatic system, *Journal of Geophysical Research*, v. 99, no. B3, p. 4341-4354.

Moran, S. C., Malone, S. D., Qamar, A. I., Thelen, W. A., Wright, A. K., Caplan Auerbach, J., in press, Seismicity associated with renewed dome building at Mount St. Helens, 2004-2005, ch. 2, *In Sherrod, D. R., Scott, W. E., and Stauffer, P. H., eds., A volcano rekindled: the renewed eruption of Mount St. Helens, 2004-2006*: U. S. Geological Survey Professional Paper.

Mullineaux, D. R. and Crandell, D. R., 1981, The Eruptive History of Mount St. Helens. *In: Lipman, P., Mullineaux, D. (Eds.), The 1980 Eruptions of Mount St. Helens, U.S. Geological Survey Professional Paper*, v. 1250, p. 3-15.

Nikon corporation, 2007, URL: http://www.nikon.com, accessed August 25, 2007.

Pallister, J. S., Hoblitt, R. P., Crandell, D. R., Mullineaux, D. R., 1992, Mount St. Helens a decade after the 1980 eruptions: magmatic models, chemical cycles, and a revised hazards assessment, *Bulletin of Volcanology*, v. 54, no. 2, p. 126-146.

Pedersen, R., Sigmundsson, F., 2004, InSAR based sill model links spatially offset areas of deformation and seismicity for the 1994 unrest episode at Eyjafjallajoekull volcano, Iceland, *Geophysical Research Letters*, v. 31, no. 14, L14610.

Poland, M., Burgmann, R., Dzurisin, D., Lisowski, M., Masterlark, T., Owen, S., Fink, J., 2006a, Constraints on the mechanism of long-term, steady subsidence at Medicine Lake volcano, northern California, from GPS, leveling, and InSAR, *Journal of Volcanology and Geothermal Research*, v. 150, p. 55-78.

Poland, M., Hamburger, M., Newman, A., 2006b, The changing shapes of active volcanoes: History, evolution, and future challenges for volcano geodesy, *Journal of Volcanology and Geothermal Research*, v. 150, p. 1-13.

Pyle, E., Elliott, J., 2006, Quantitative morphology, recent evolution, and future activity of the Kameni Islands volcano, Santorini, Greece, *Geosphere*, v. 3, no. 5, p. 253 268.

Remondino, F. and El-Hakim, S., 2006, Image-based 3D modeling: A review, *The Photogrammetric Record*, v. 21, p. 269-291.

Scarpa, R., Tilling, R. I., 1996, Monitoring and mitigation of volcano hazards, *Springer Verlag*, New York, Secaucus, NJ (USA).

Schilling, S. P., Carrara, P. E., Thompson, R. A., Iwatsubo, E. Y., 2004, Posteruption glacier development within the crater of Mount St. Helens, Washington, USA, *Quaternary Research*, v. 61, p. 325-329.

Schilling, S. P., Thompson, R. A., Messerich, J. A., Iwatsubo, E. Y., in press, Use o digital vertical aerophotogrammetry to determine rates of lava dome growth, Mount St. Helens, 2004-2005, *In Sherrod, D. R., Scott, W. E., and Stauffer, P. H., eds., A volcano rekindled: the renewed eruption of Mount St. Helens, 2004-2006*: U. S. Geological Survey Professional Paper.

Scott, W. E., Sherrod, D. R., Gardner, C. A., in press, Overview of the 2004 to 2005, and continuing, eruption of Mount St. Helens, Washington, *In Sherrod, D. R., Scott, W. E., and Stauffer, P. H., eds., A volcano rekindled: the renewed eruption of Mount St. Helens, 2004-2006*: U. S. Geological Survey Professional Paper.

Sherrod, D., Smith, J. G., 1990, Quaternary extrusion rates of the Cascade Range, Northwestern United States and southern British Columbia, *Journal of Geophysical Research*, v. 95, p. 465-474.

Stevens, N. F., 2002, Emplacement of the large andesite lava flow in the Oturere Stream valley, Tongariro Volcano, from airborne interferometric radar, *New Zealand Journal of Geology and Geophysics*, vol. 45, p. 387-394.

Stoer, J. and Bulirsch, R., 2002. Introduction to Numerical Analysis, *Springer*, Berlin, 673 p.

Swanson, D. A. and Holcomb, R. T., 1989, Regularities in growth of the Mount St. Helens Dacite Dome, 1980-1986, *IAVCEI Proceedings in Volcanology*, v. 2, Lava Flows and Domes.

Vallance, J. W., Schneider, D. J, Schilling, S. P., in press, Growth of the 2004-2006 dome complex at Mount St. Helens, ch. 9, *In Sherrod, D. R., Scott, W. E., and Stauffer, P. H., eds., A volcano rekindled: the renewed eruption of Mount St. Helens, 2004-2006*: U. S. Geological Survey Professional Paper.

Thompson, R. A., Schilling, S. P., 2007, Photogrammetry, *in* Dzurisin, D., ed., Volcano deformation – geodetic monitoring techniques, , *Springer-Praxis Books in Geophysical Sciences*, Berlin, p. 195-221.

Wadge, G., 2003, Measuring the Rate of Lava Effusion by InSAR, *Proceedings of the FRINGE 2003 Workshop,* (ESA SP-550), CDROM p. 34.1

Wadge, G., Macfarlane, D. G., Robertson, D. A., Hale, A. J., Pinkerton, H., Burrell, R. V., Norton, G. E., James, M. R., 2005, AVTIS: A novel millimeter-wave ground based instrument for volcano remote sensing, *Journal of Volcanology and Geothermal Research*, v. 146, p. 307-318.

Wadge, G., Dorta, D., Cole, P., 2006, The magma budget of Volcán Arenal, Costa Rica from 1980 to 2004, *Journal of Volcanology and Geothermal Research*, v. 157, p. 60-74.

Wolf, P. R., Dewitt, B. A., 2000, Elements of photogrammetry with applications in GIS, *New York, McGraw Hill.*

Wright, R., Cruz-Reyna, S. D. L, Harris, A., Flynn, L., Gomez-Palacios, J. J., 2002, Infrared satellite monitoring at Popocatepetl: Explosions, exhalations, and cycles of dome growth, *Journal of Geophysical Research*, v. 107, no. B8.

Yokoyama, I., Seino, M., 2000, Geophysical comparison of the three eruptions in the 20th century of Usu volcano, Japan, *Earth Planets Space*, v. 52, p. 73-89.

Zlotnicki, J., Ruegg, J. C., Bachelery, P., Blum, P. A., 1990, Eruptive mechanism on Piton de la Fournaise volcano associated with the December 4, 1983, and January 18, 1984 eruptions from ground deformation monitoring and photogrammetric surveys, *Journal of Volcanology and Geothermal Research*, v. 40, no. 3, p. 197 217.
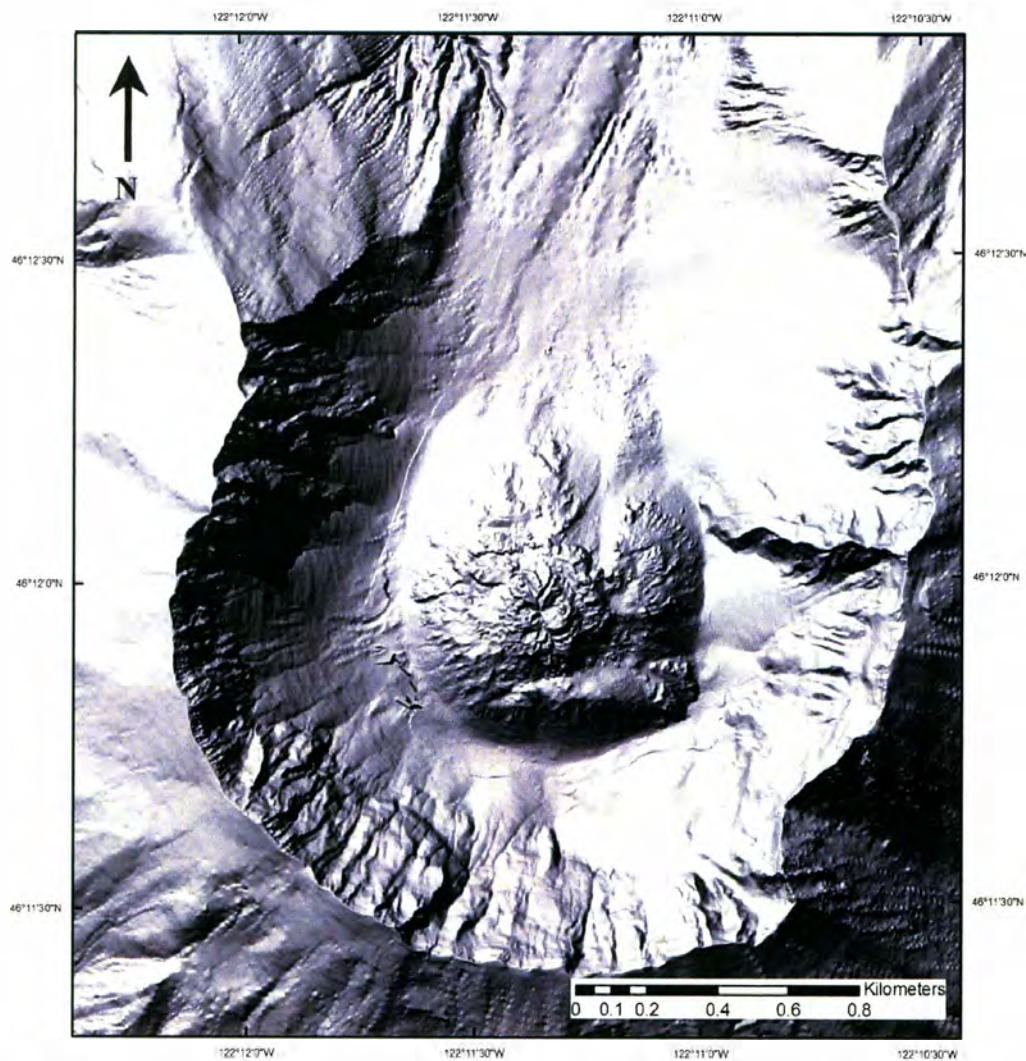
Figure 1. A. Location of Mount St. Helens volcano in southwestern Washington State. Black box represents approximate location of Mount St. Helens. **B.** Close-in view of 1986 DEM of the volcano shows the 1980-1986 Dome in the center of the horse-shoe crater.

Figure 2. Nikon D70 digital single-lens reflex (SLR) camera used for oblique photogrammetry (Nikon, 2007).
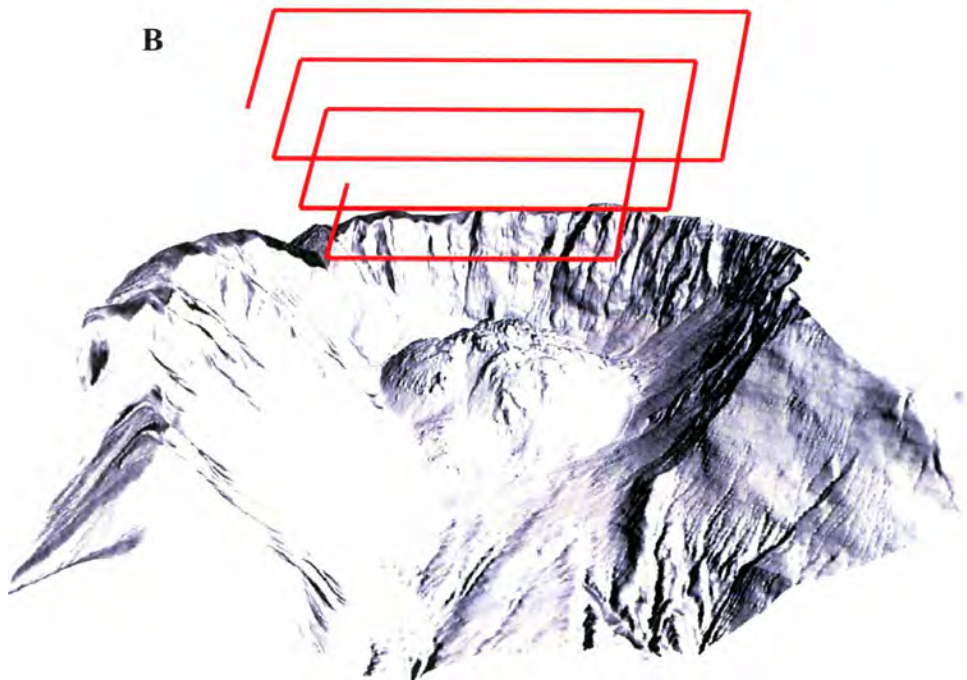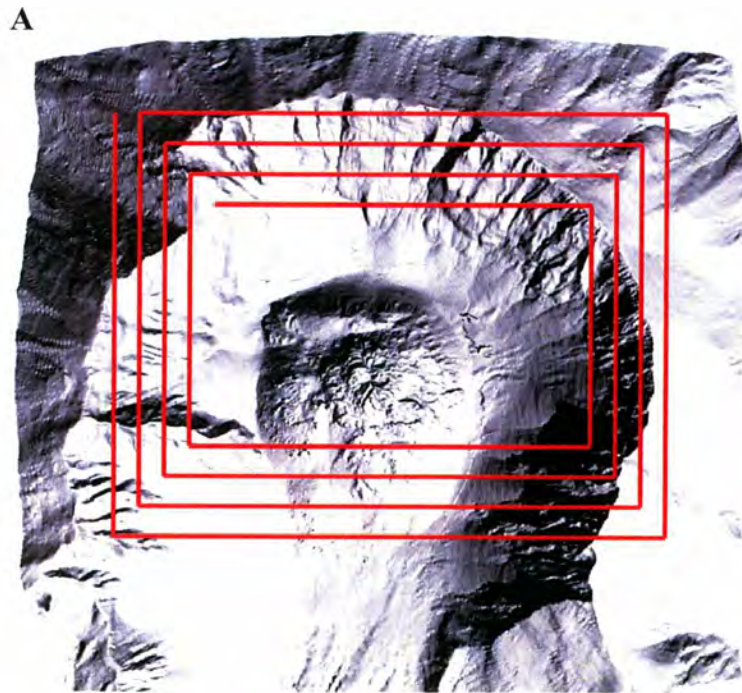
Figure 3. Schematic representation of a typical helicopter flight path (in red), vertical (**A**) and perspective view (**B**), during acquisition of oblique photographs at Mount St. Helens.
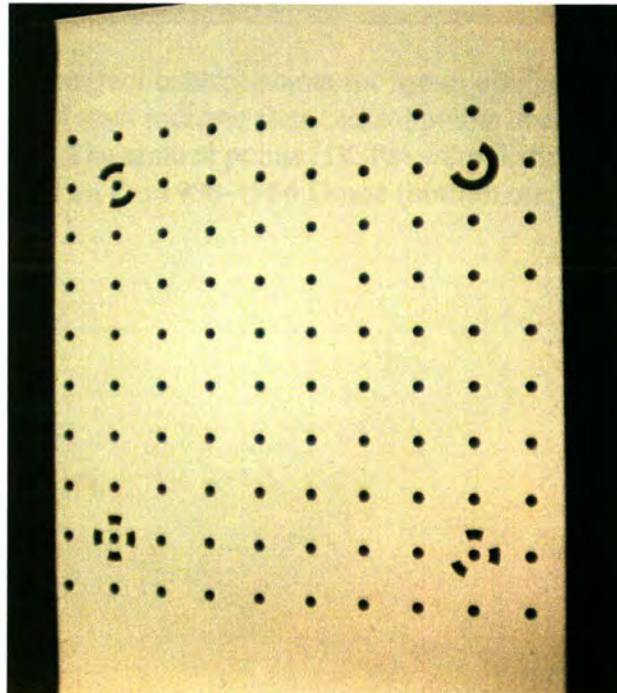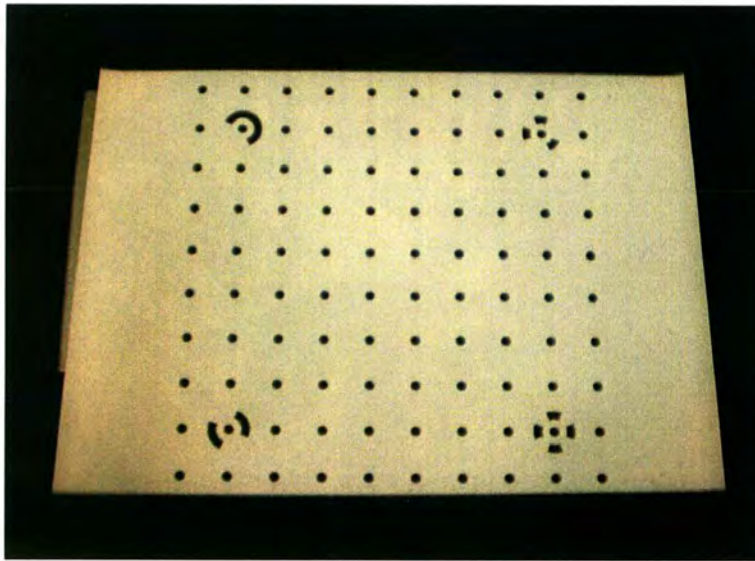
Figure 4. Calibration target grids provided by PhotoModeler Inc. used for camera calibration. The target grid was shot at four locations in both landscape and portrait views with the Nikon D70 used to acquire oblique photographs of Mount St. Helens.
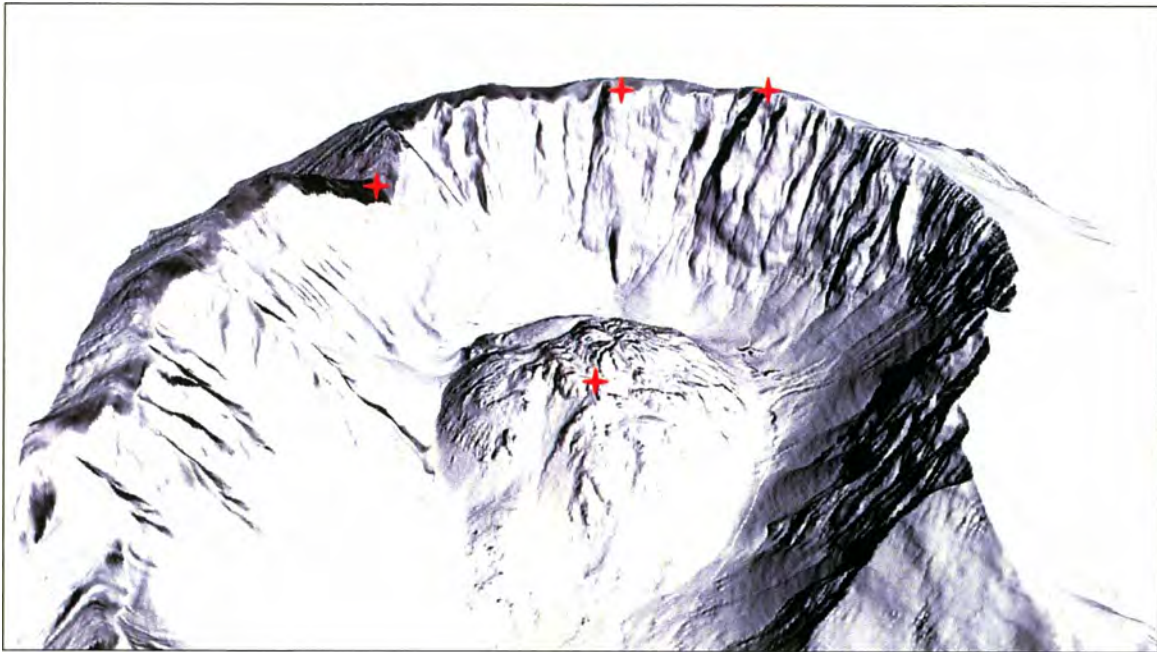
Figure 5. DEM used to extract control points for use in oblique photogrammetry processing methods. Red stars indicate four control points used in every oblique photogrammetry model. The control points (GCPs) were distinctive features on the crater rim (top three) and on the 1980-1986 Dome (bottom one).
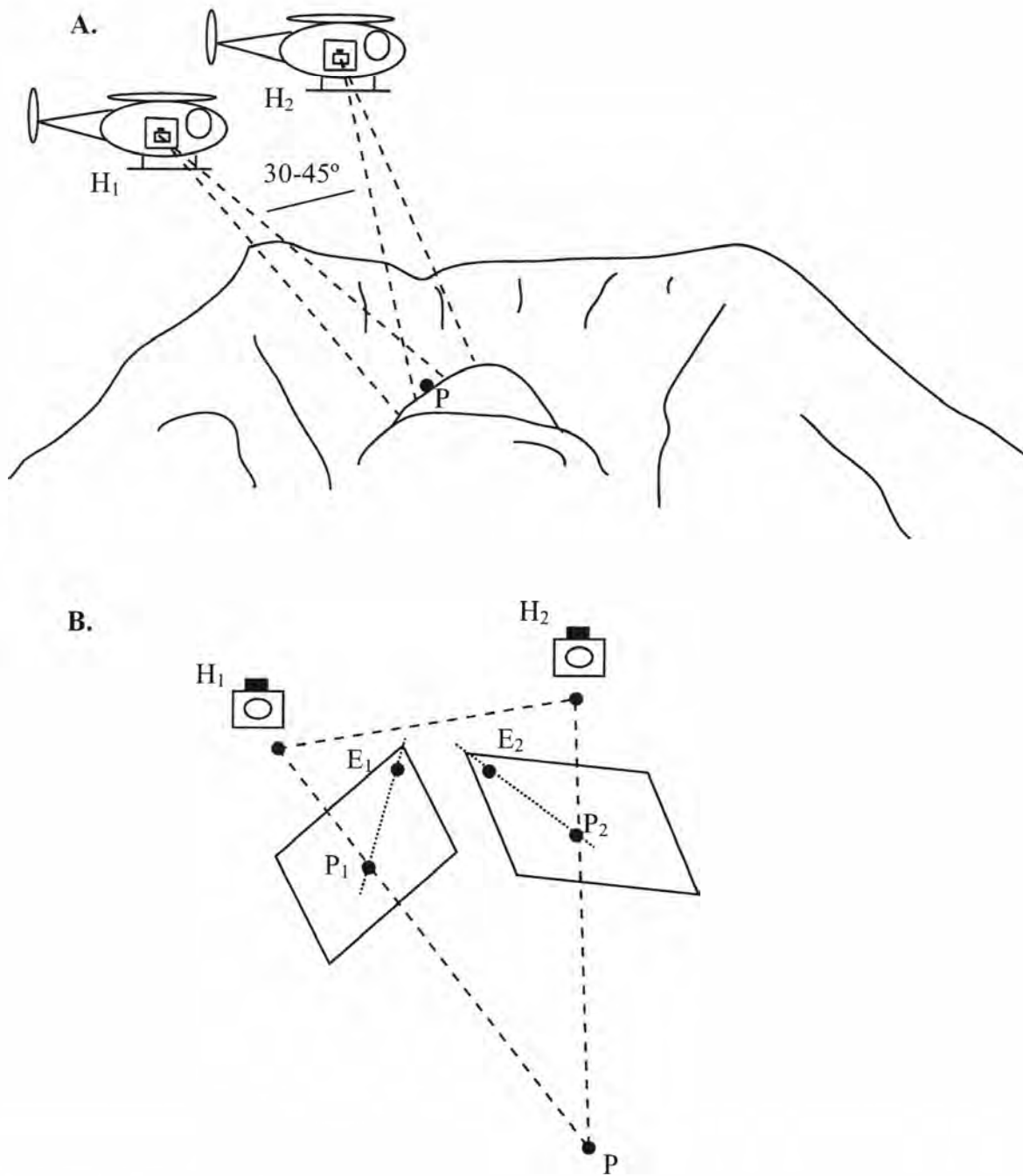
Figure 6. Example of overlapping oblique photographs and epipolar geometry. Two cameras, with their respective focal points H_1 and H_2, observe a point P on the 2004-2007 Dome at Mount St. Helens (**A**). The projection of P onto each of the image planes is denoted P_1 and P_2. Points E_1 and E_2 are the epipoles. The line H_2-P is seen by the H_2 camera as a point because it is directly in line with that camera's focal point. However, the H_1 camera sees this line as a line in its image plane. That line (H_2-P) in the H_1 camera is called an epipolar line (**B**).
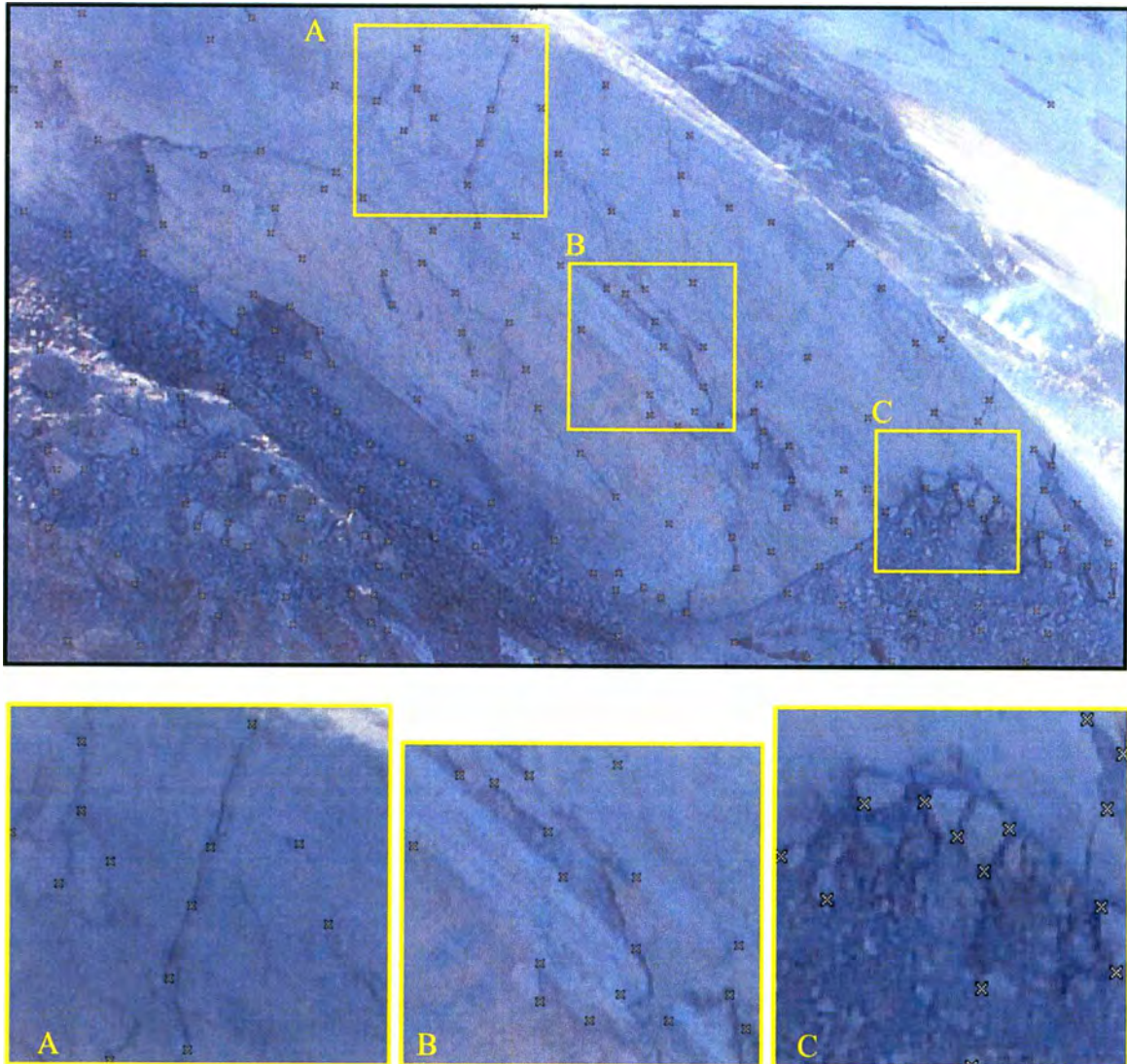
Figure 7. Reference points represented by white crosses located on the dome. Reference points were easily identifiable features located on the 2004-2007 dome, which included intersection of cracks (**A**), striae (**B**), and edges of large talus (**C**). Photograph taken on 2/22/2005 by Steve Schilling, USGS.

A
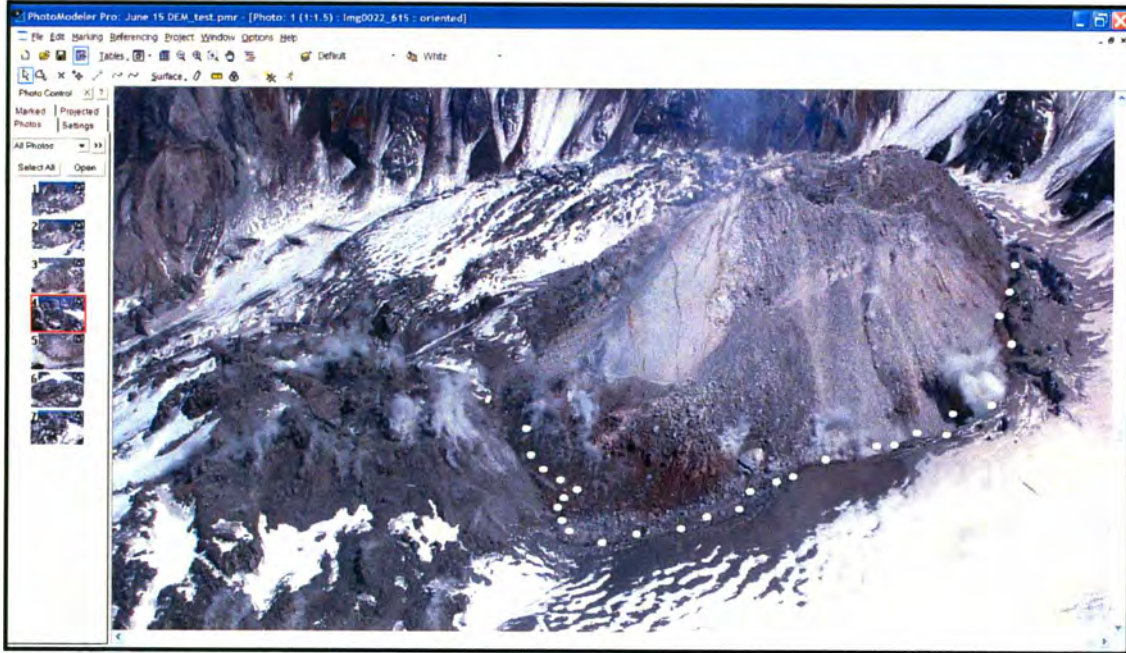
B
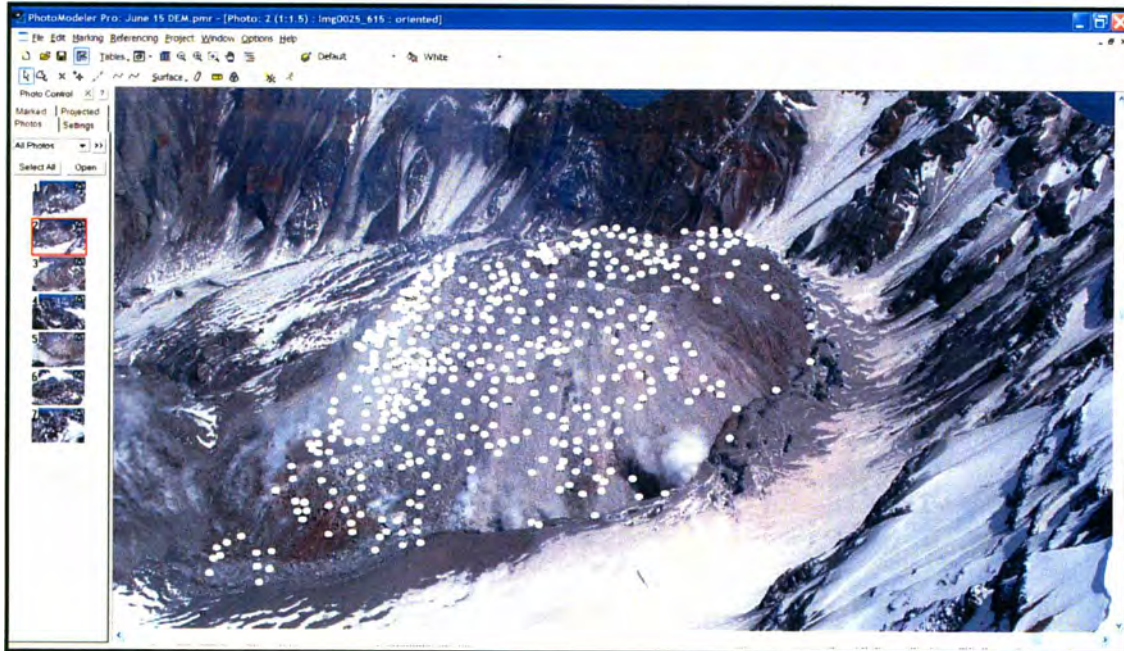
Figure 8. **A.** Screen capture from PhotoModeler of oblique photographs taken on June 15, 2005. White dots were overlain on small white crosses to illustrate the placement of points that are used to build a perimeter of extruded lava. **B.** Example of a point cloud, where points (white dots) are located in two or more oblique photographs. Each photograph illustrates a point perimeter or point cloud from one vantage point in a set of oblique photographs used to build a DEM.
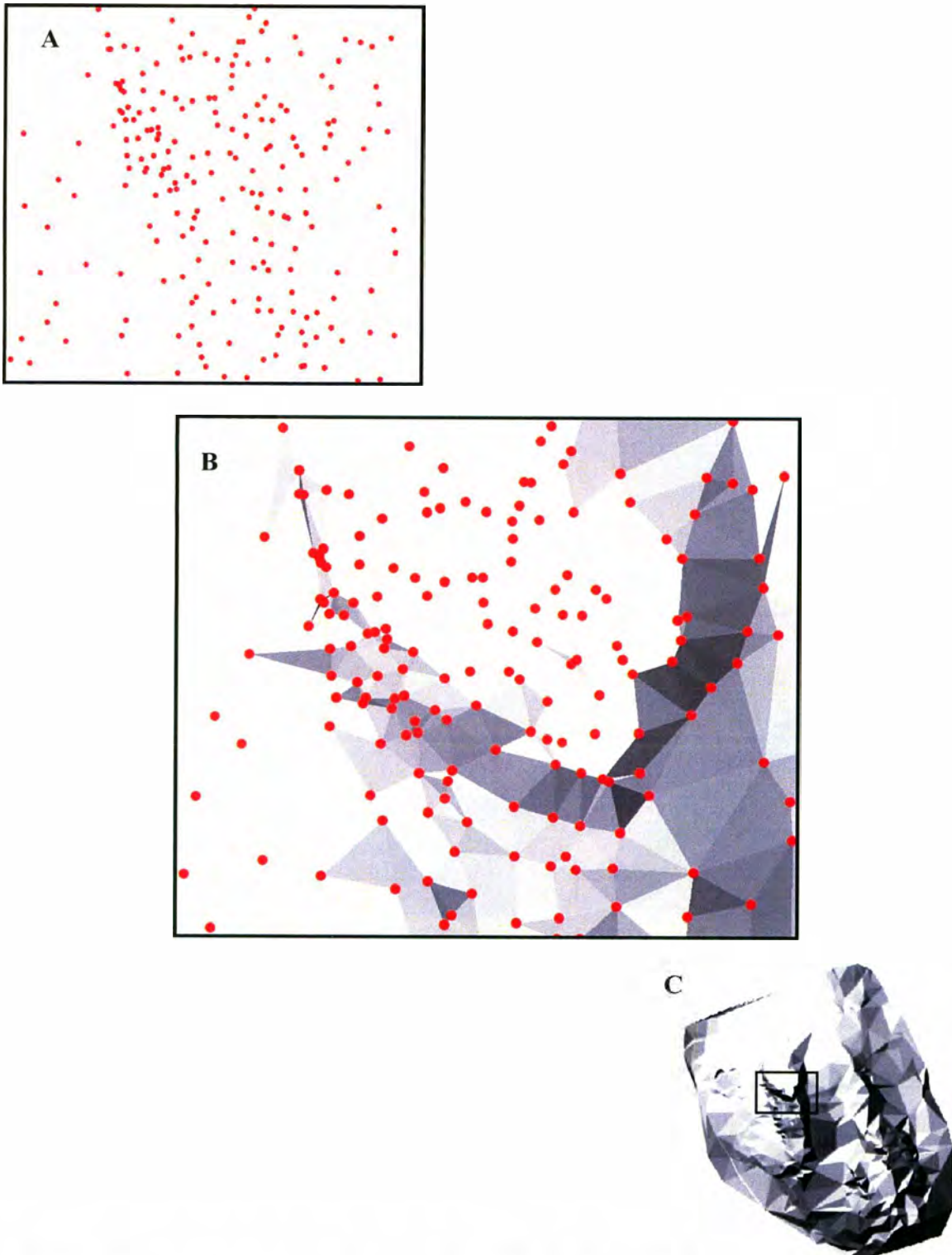
Figure 9. Triangulated irregular network (TIN) production. Nodes (x, y, z) are added to a GIS (**A**), the nodes are connected by lines, edges and triangles to their nearest neighbor (**B**), these triangles represent the surface of the model, which is eventually converted to a raster digital elevation model DEM for volume calculations (**C**).

Figure 10. **A.** Illustration of volume calculated using a flat plane projected from the lowest elevation point on the oblique DEM (grey). Volumes calculated this way substantially underestimate the volume of new material added on top of the 1986 surface (blue). **B.** Volume calculations using the 1986 pre-eruption surface as a baseline. This type of volume calculation projects vertical walls downward from the perimeter of the oblique DEM (grey) to the 1986 surface (blue). The varying topography of the 1986 baseline surface is evident in the profile view (bottom left).

81
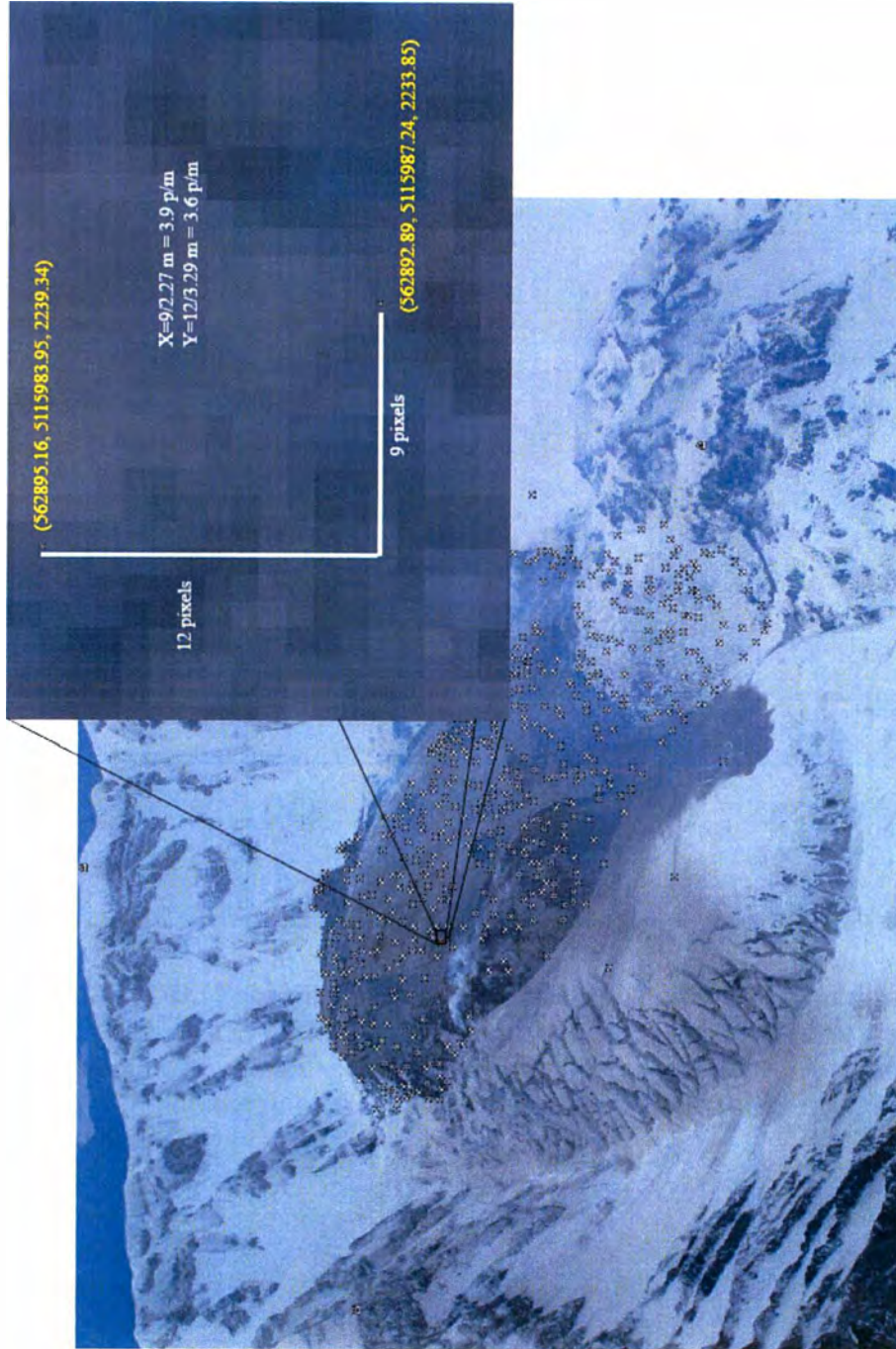
Figure 11. Oblique aerial photograph taken 4/10/05 from altitude of 2717m. The view is looking south-southwest. White crosses indicate points selected in photos for DEM creation. Inset shows an enlarged view of a small area of the image. Coordinates of the endpoints of two lines are given, as are the number of pixels along each line. These values are used to estimate the GSD at this location in the image. In this case, the pixel ground sample distance is roughly equal to 0.26m. This measurement indicates that the horizontal distance captured in this image is nearly 0.8 km, a good representation of the length of landscape of this particular image.
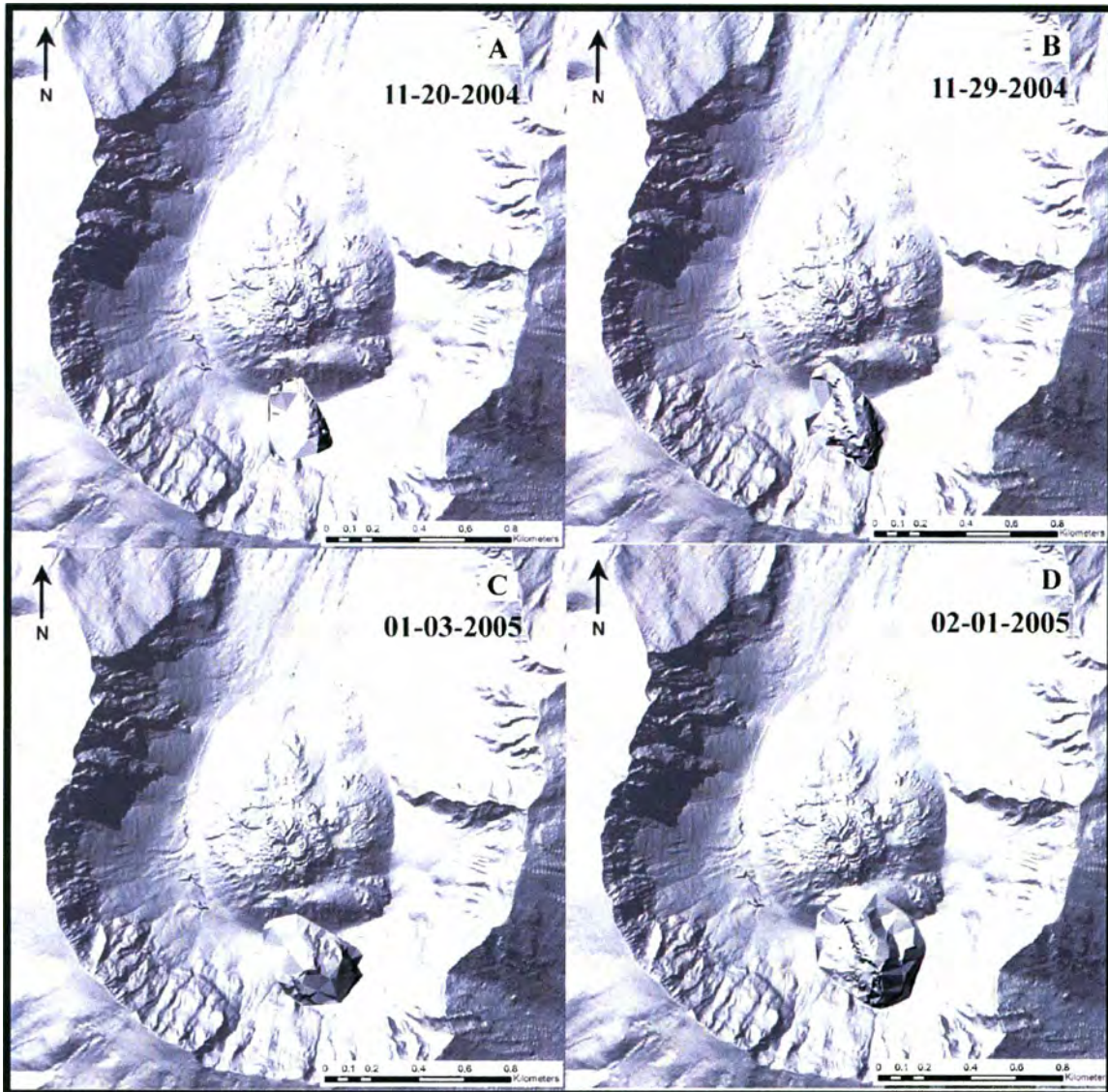
Figure 12 A-D. Sequence of twelve DEMs (A-L) produced by oblique photogrammetry overlain on a USGS DEM from 1986 derived by means of vertical aerial photogrammetry. Dates span November 2004 to April 2007. A similar set of images of vertical aerophotogrammetric DEMs can be seen in Schilling et al., (*in press*). Continued on the next page.

Figure 12. Continued.
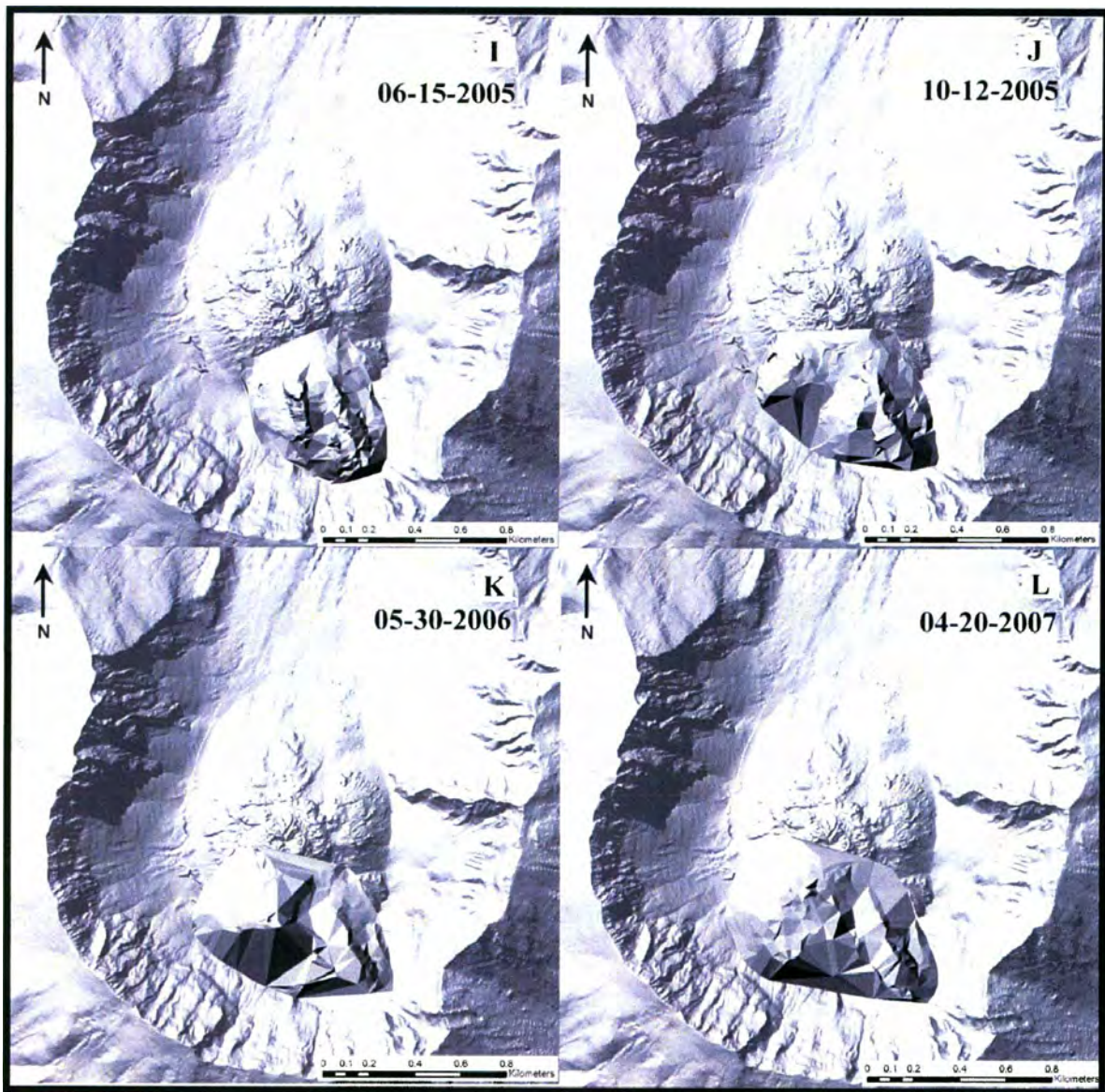
Figure 12. Continued.
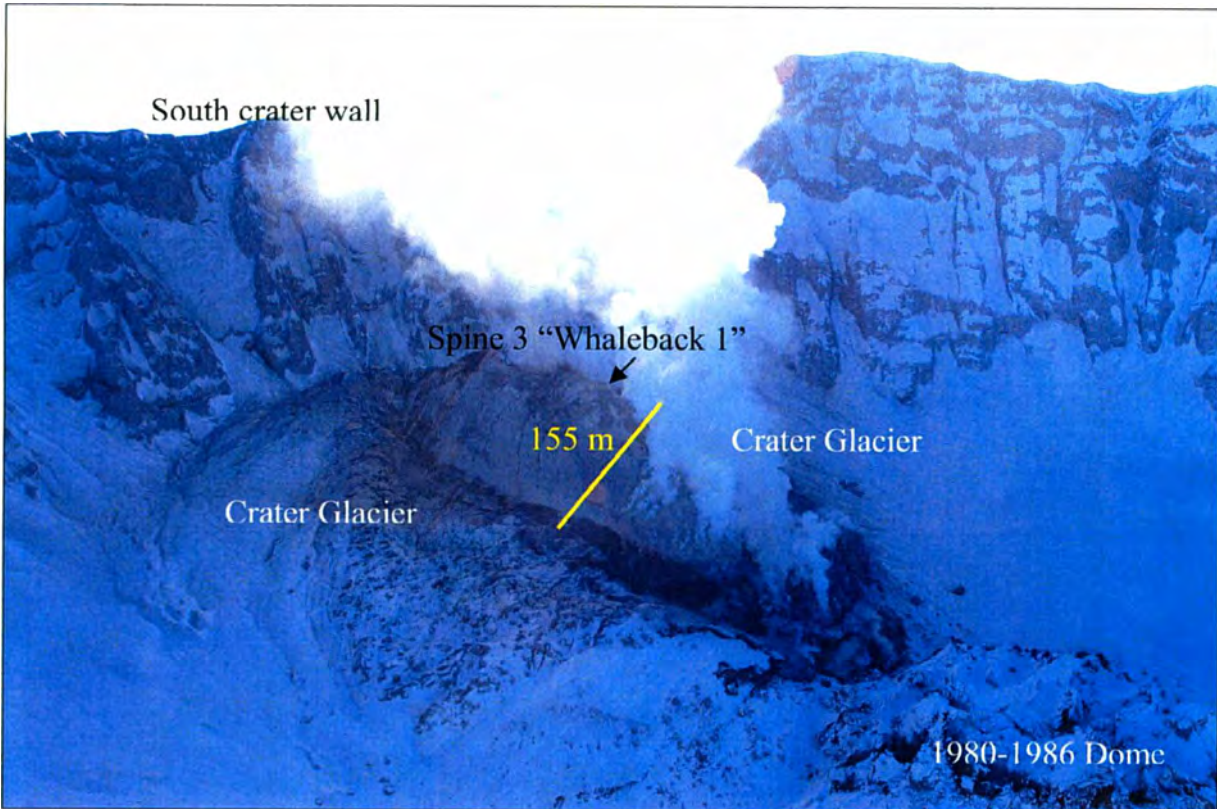
Figure 13. Oblique photograph taken November 20, 2004. Growth of Spine 3 directly south of 1980-1986 Dome, breaking through Crater Glacier as a solid dacite plug.
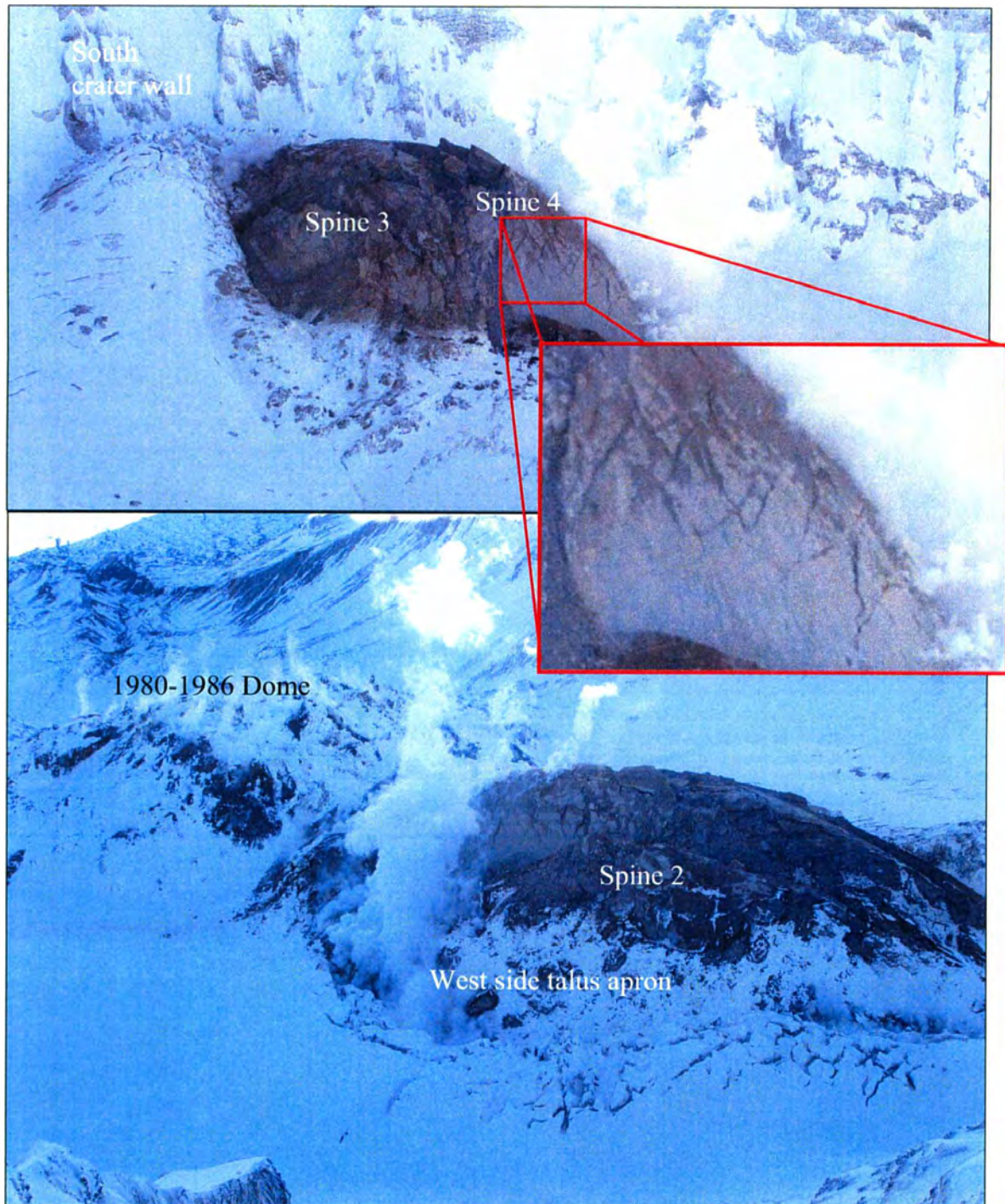
Figure 14. January 3, 2005 oblique photographs. Emergence of Spine 4, overthrusting Spine 2 and 3. Talus aprons began forming at this time predominantly on the west side of the dome. Typical features of spines, which include gouge, striae, discoloration and large cracks are highlighted in the red box.
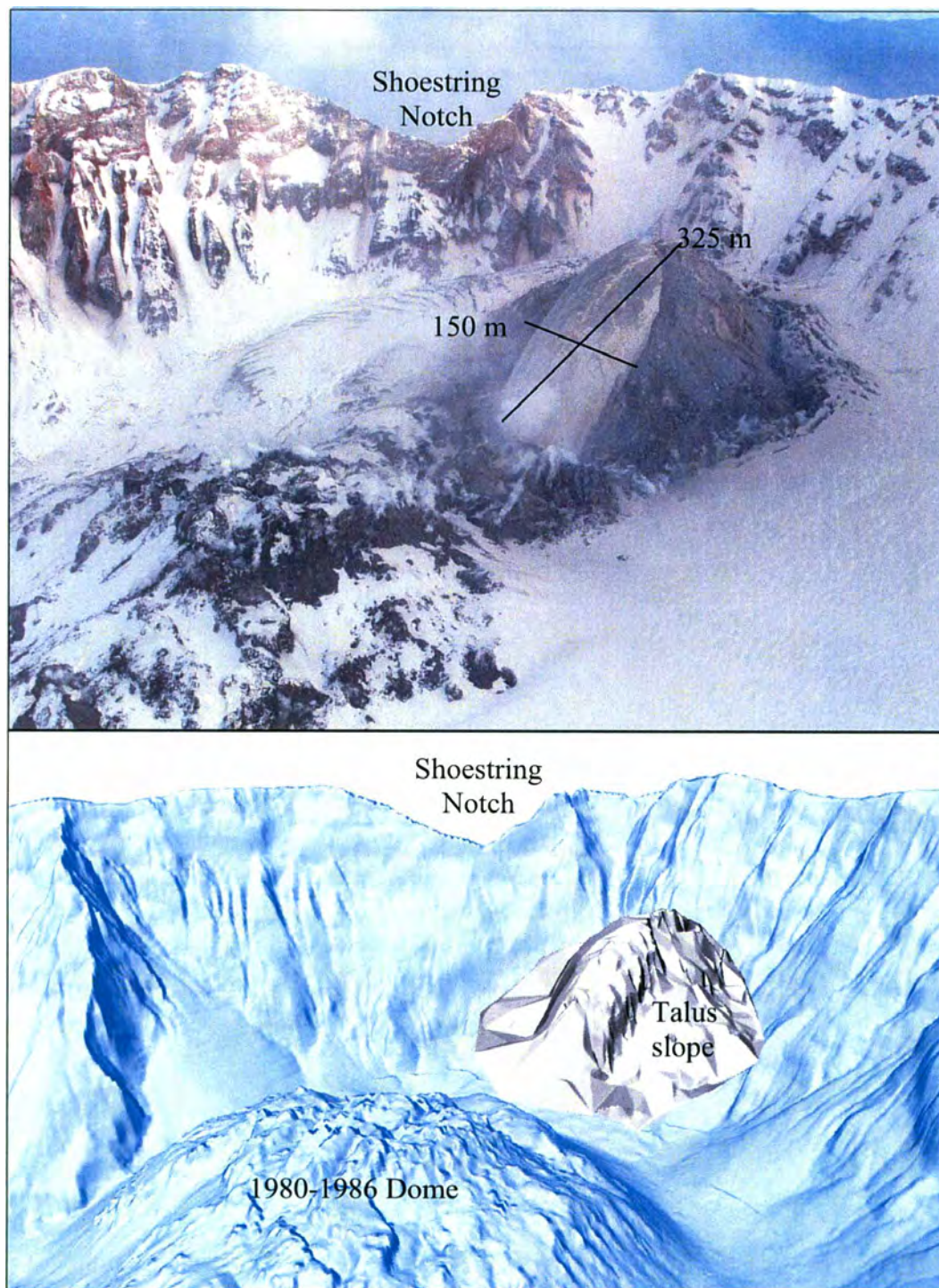
Figure 15. Southeast view of February 1, 2005 oblique photograph (above) associated DEM (below, gray scale). Cylindrical-like body is easily noticeable at this date. 1986 DEM is shown in blue as a reference frame for oblique photography DEM. Oblique DEM appears to float above the 1986 surface because the surrounding glacier that masks the 2004-2007 surface was not modeled.
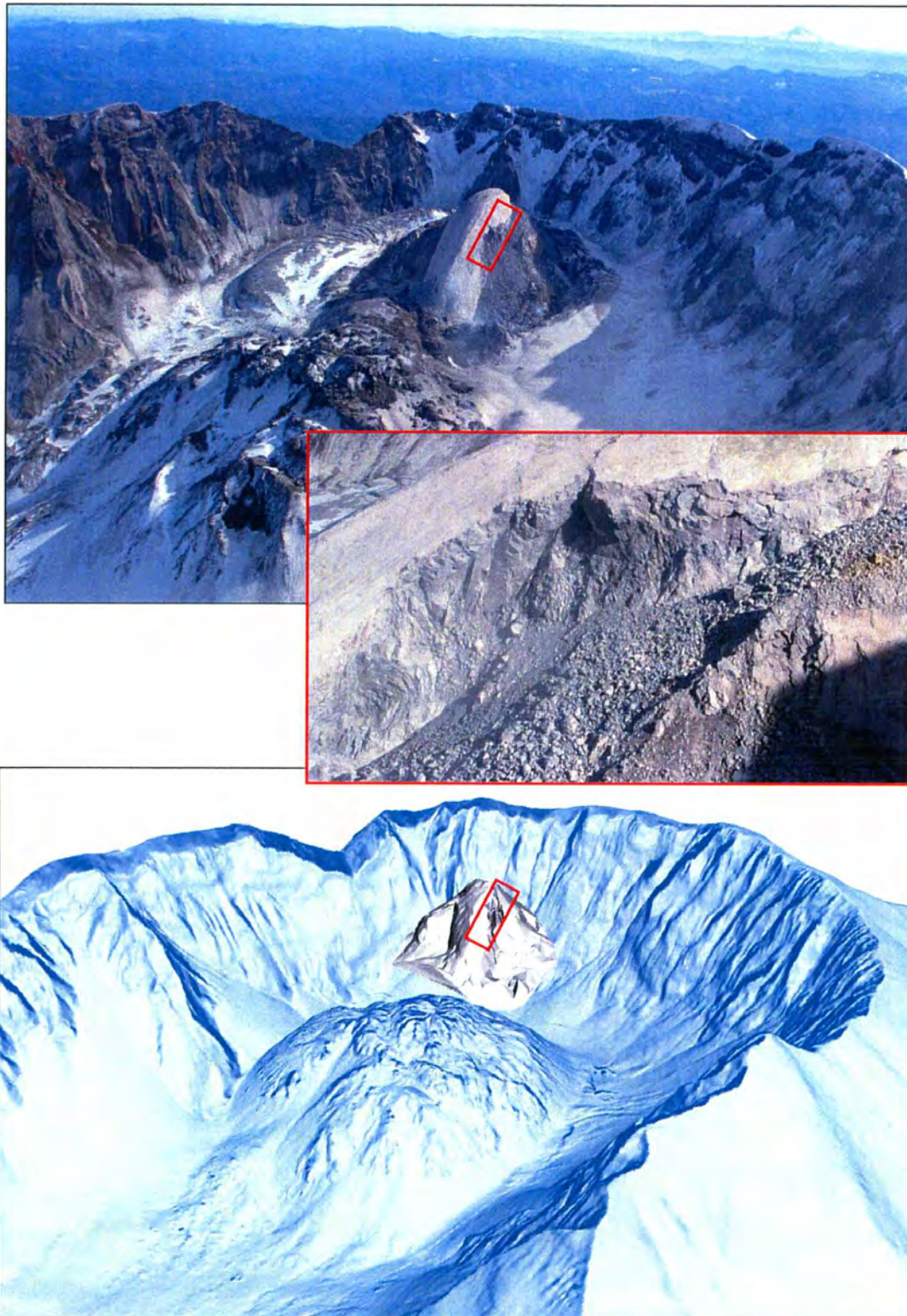
Figure 16. February 22, 2005 oblique photograph (above) and associated DEM (below in gray scale, merged with 1986 DEM in blue) looking south-southeast toward the growing dome inside the crater of Mount St. Helens. Red rectangles on each image represent approximate area of a large section of spine collapse (middle).
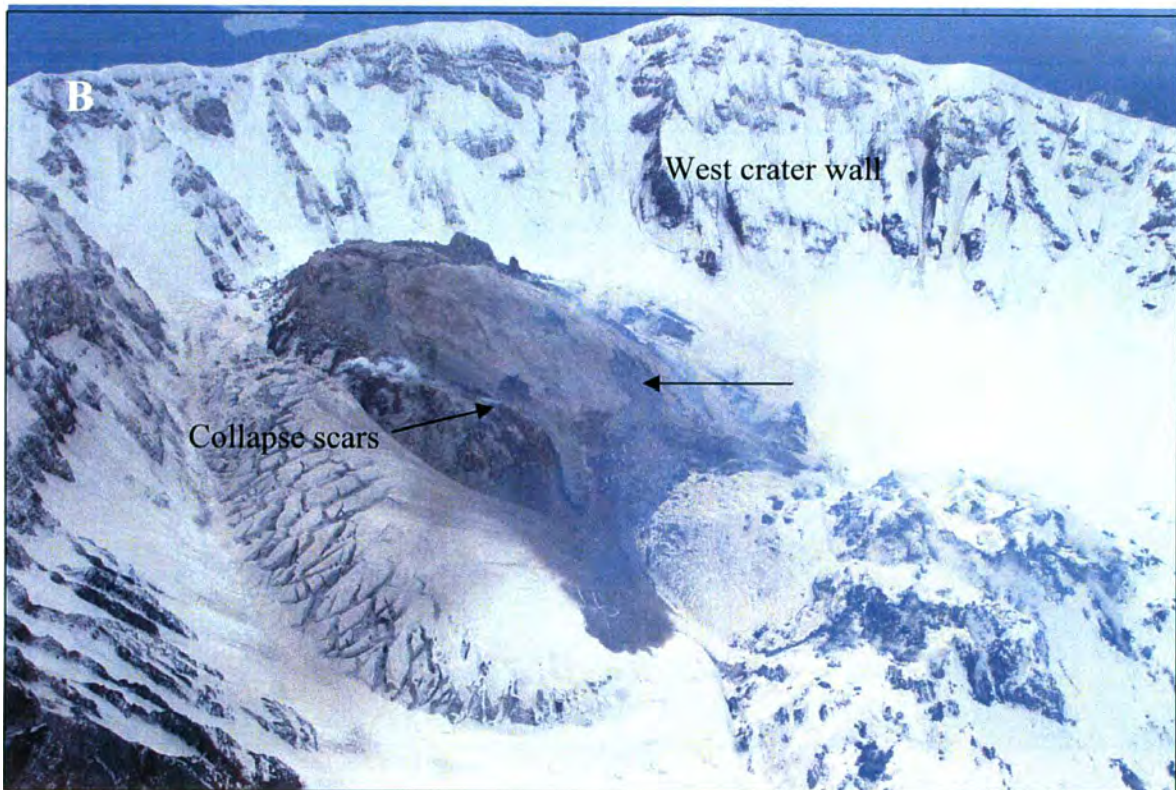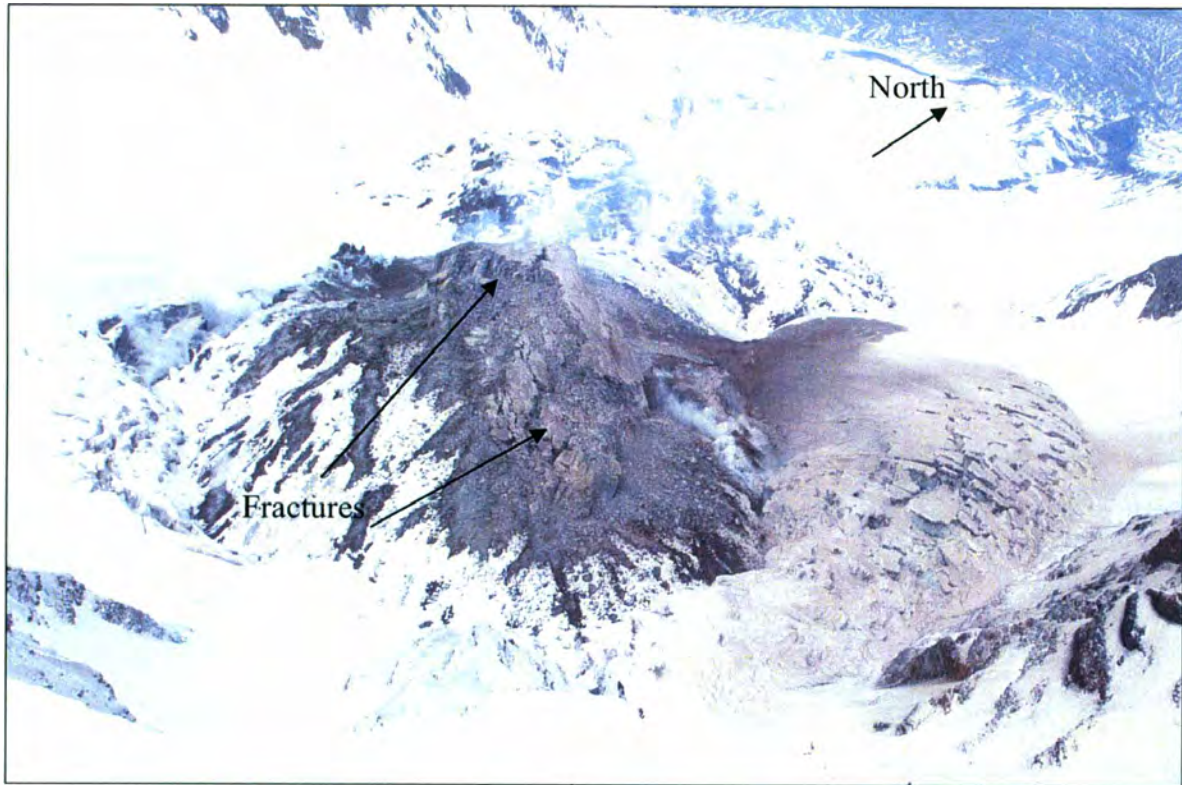
Figure 17. April 10, 2005 oblique photographs of Spine 4, several fractures (A) and large collapse scars (B) formed by the onset of disintegration of Spine 4.
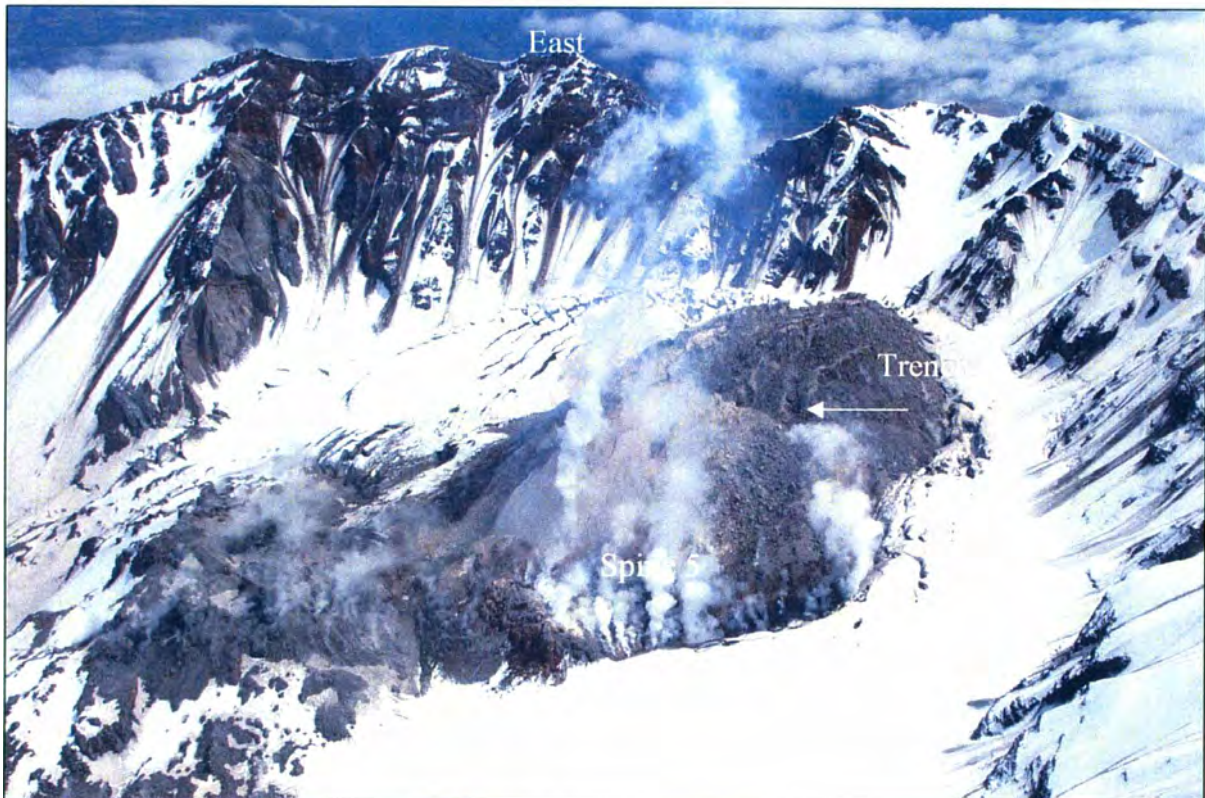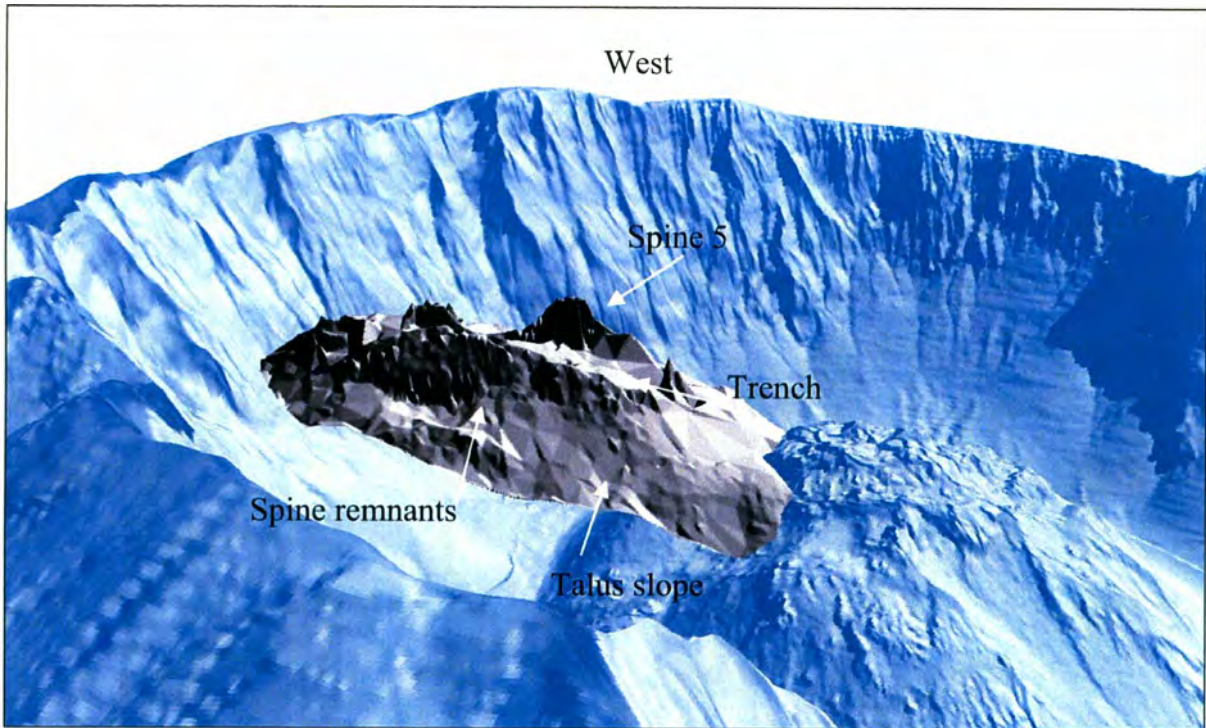
Figure 18. Oblique photogrammetry DEM (above) and photograph (below) acquired May 12, 2005. The emergence of Spine 5 marks westward migration of dome growth. A talus trench is located between the Spine 5 and the remnants of previous spines.

Figure 19. October 12, 2005 oblique photograph taken northeast of the growing dome by helicopter. Succession of spines can be seen as the locus of growth migrated over 200 m to the west at this date. Alternations of exogenous and endogenous growth produce Spine 6.
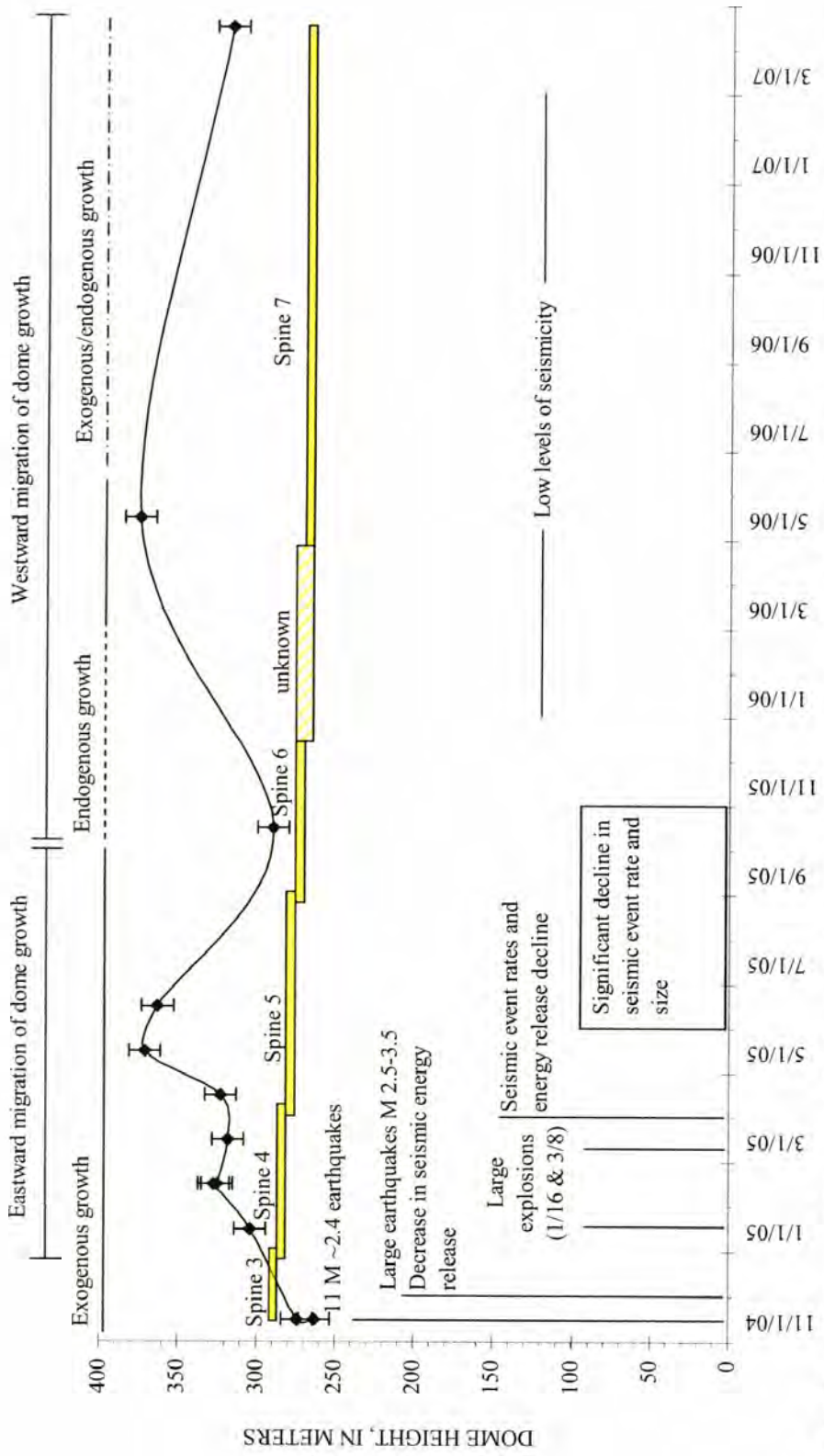
Figure 20. Time-series of dome height through time and significant seismic, deformation, and collapse events (Moran et al., *in press*; Schilling et al., *in press*). Dome heights were measured using the oblique DEMs. Height measurements have a 10 m error bar, a maximum estimate of the height difference between oblique DEM and vertical aerophotogrammetry DEMs.

93
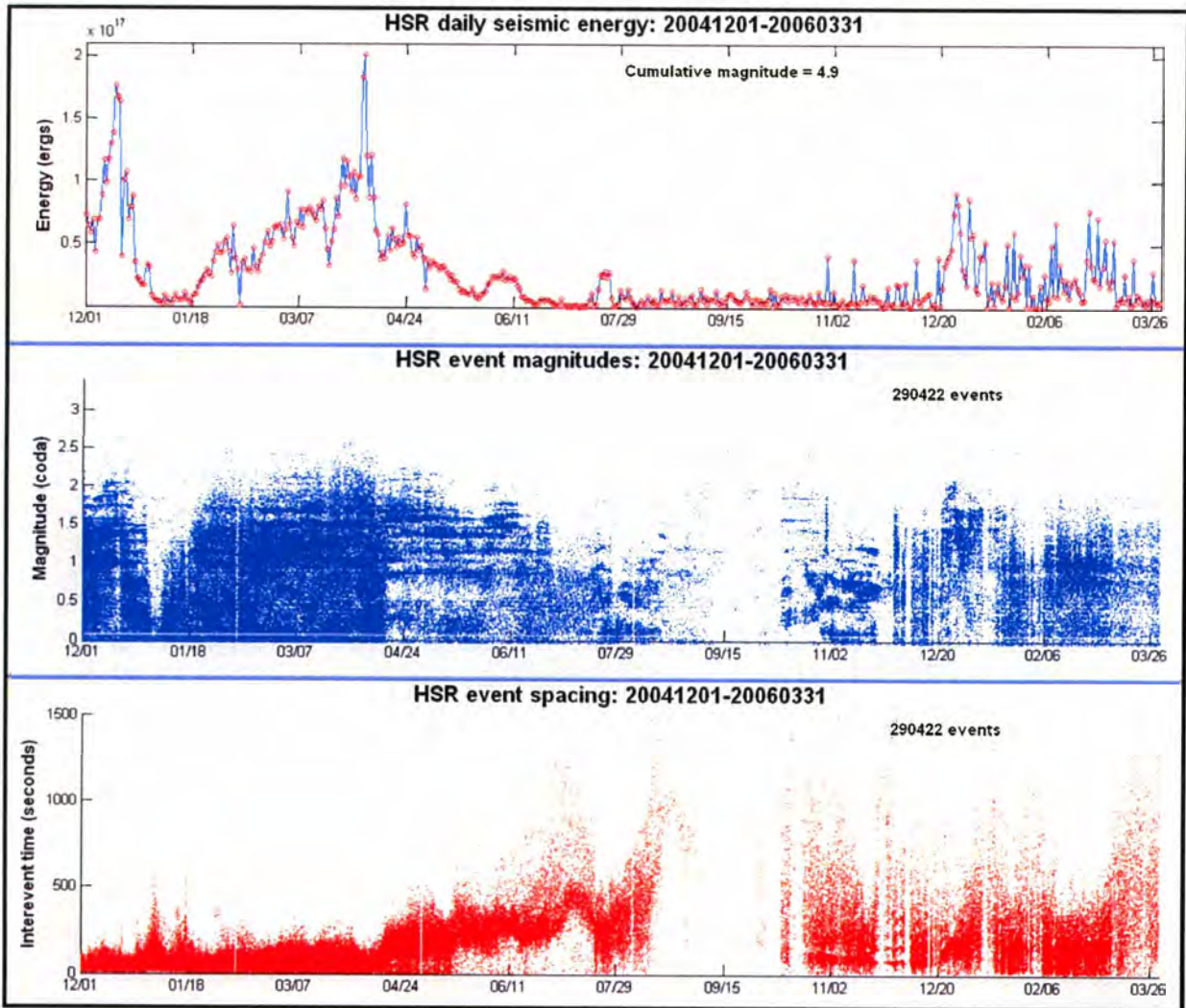
Figure 21. Seismic plots of event magnitudes and spacing, and resultant daily seismic energy estimates for December 2004 - March 2006 (Moran et al., *in press).*

Figure 22. Total dome volume and extrusion rate calculations made from oblique photogrammetric DEMs through time at Mount St. Helens. Dashed black line represents the break between rapid dome volume accumulation and much varied extrusion rates to a gentler slope in volume accumulation and relatively steady extrusion rates. There are two extrusion rate values for the date of 11/29/2004, see Table 6.
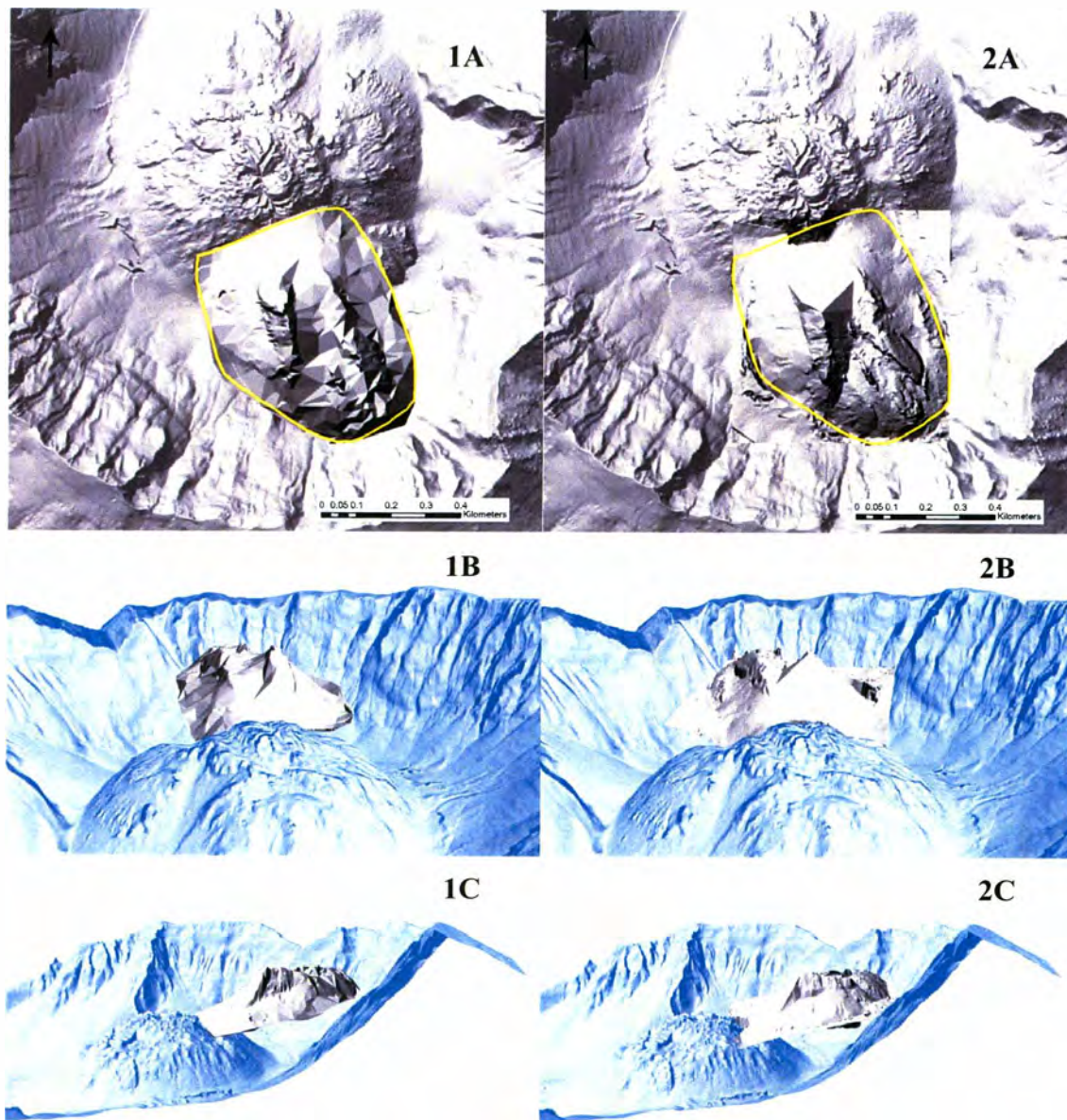
Figure 23. An example of qualitative comparison between DEMs derived by means of oblique photogrammetry (1A-C) and DEMs derived by vertical aerophotogrammetry (2A-C). Images 1A and 2A show typical vertical view of the dome on June 15, 2005, extruded rock perimeter is outlined in yellow. Images 1B and 2B are three-dimensional views looking south at the dome with the 1980-1986 Dome in the foreground. Images 1C and 2C are profile views looking east with the west crater wall clipped to allow full view of the DEMs.
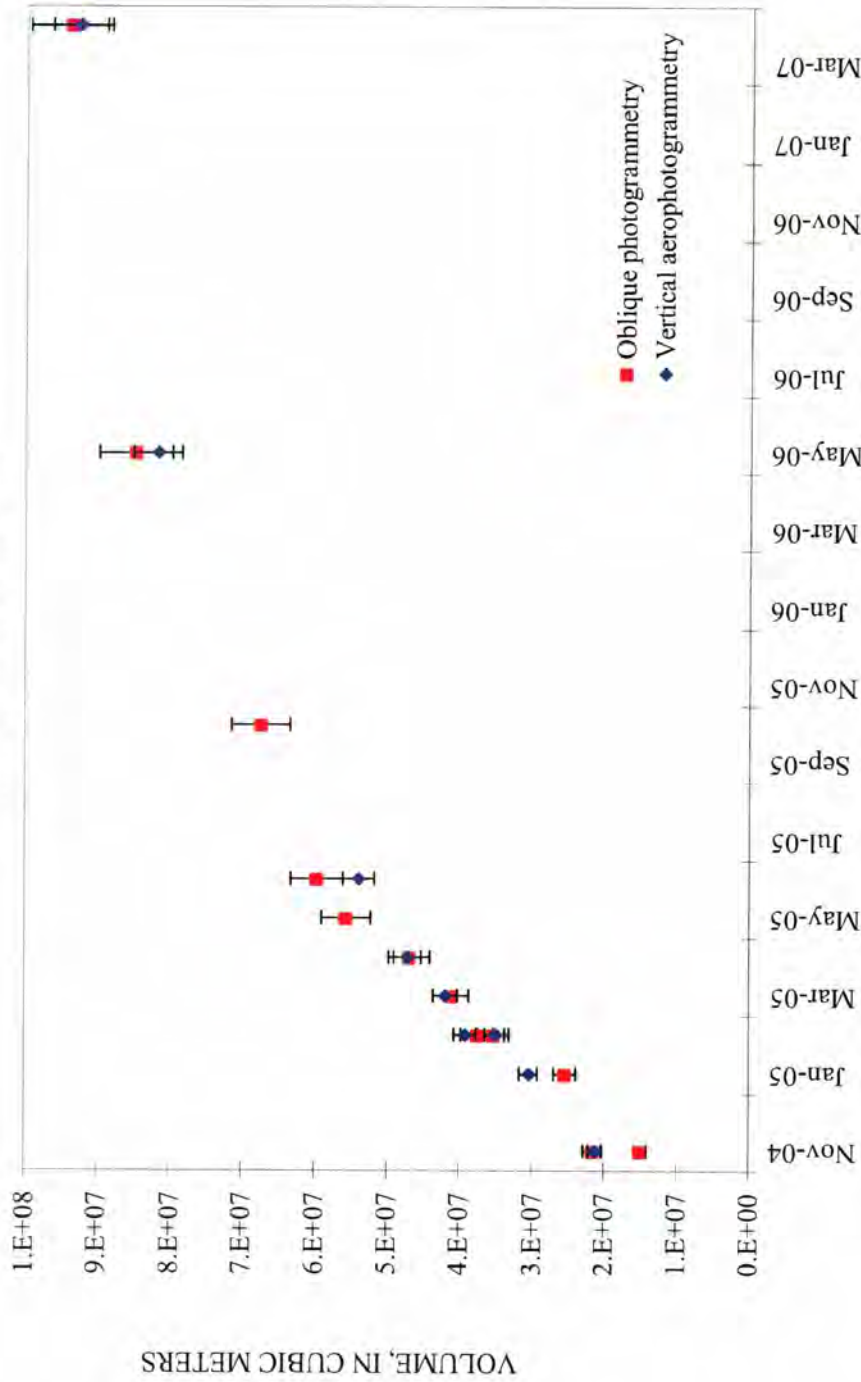
Figure 24. Total dome volumes calculated from DEMs made by oblique photogrammetry and vertical aerophotogrammetry methods. Associated estimated volume uncertainty represented by error bars of 9% and 4% respectively. Volume estimates made by both techniques fall within the error or each other, with the exception of January 3, 2005. Note that vertical aerophotogrammetry surveys were not deployed on 11/20/2004, 5/12/2005 and 10/12/2005.
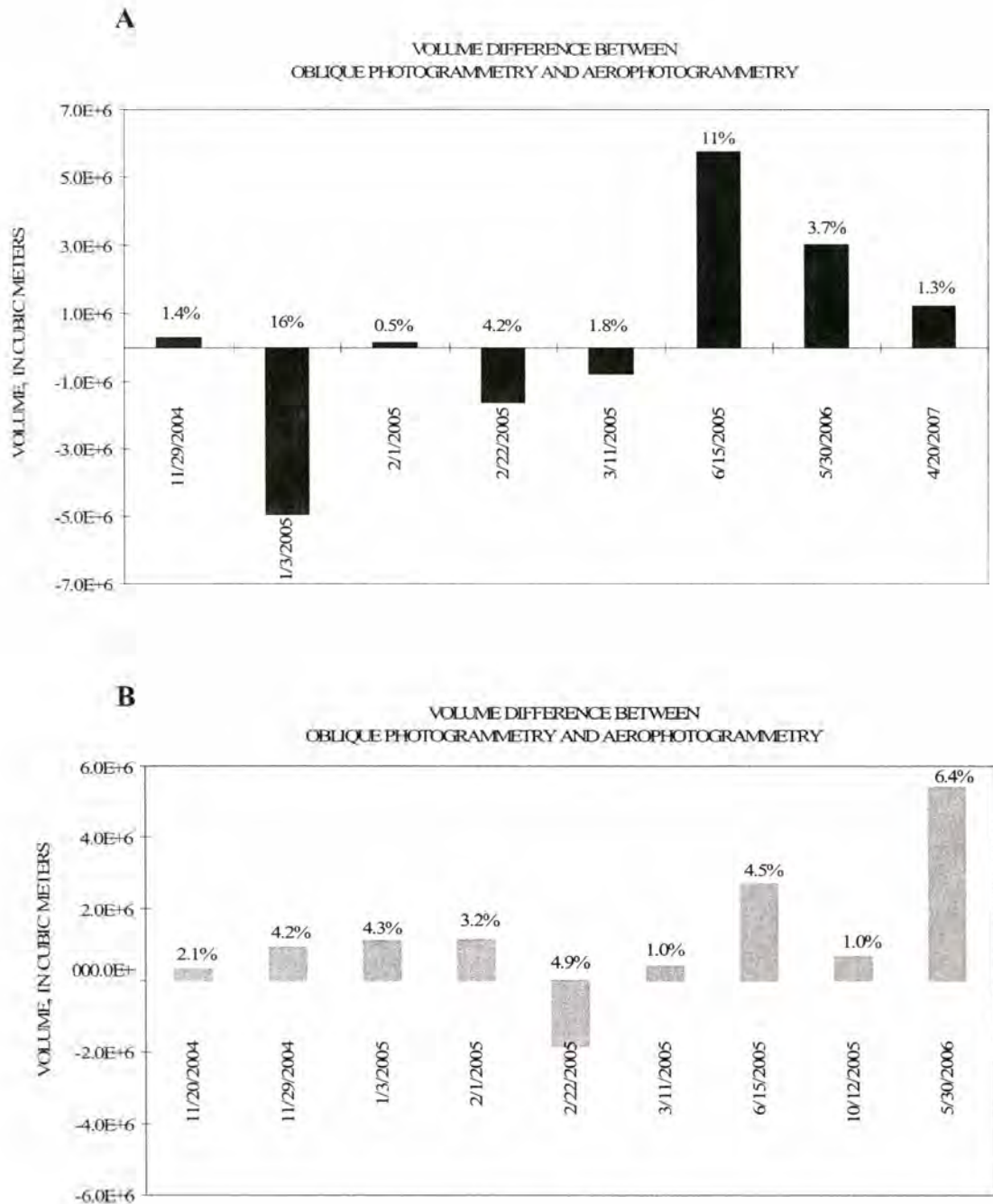
Figure 25. A. Volumetric calculation differences (black bars) represented by variations in DEMs derived by different techniques. Associated percent difference is labeled above each bar. **B.** Calculated volume differences (gray bars) by oblique photogrammetry and vertical aerophotogrammetry techniques using the same clipping boundary of the growing dome. Percent difference values for each date are listed above volume difference bars.
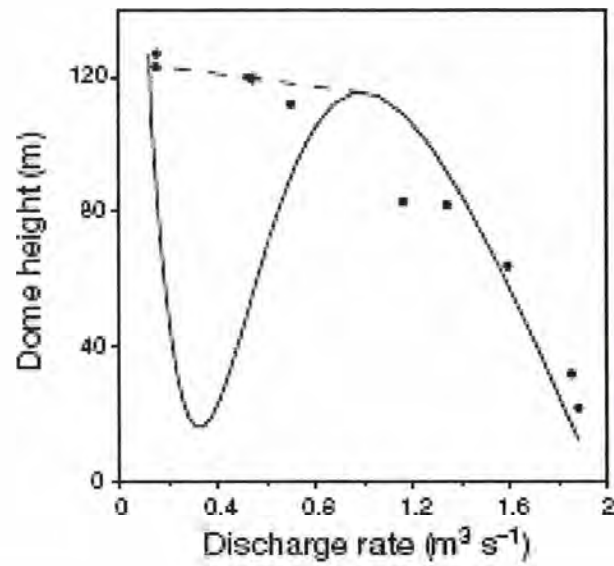
Figure 26. Calculated and observed magma discharge rate versus dome height. Filled circles represent measurements of dome height in October 1997 at Sourfriere Hills volcano. The solid line represents a steady state. The dashed line shows a change from one eruptive state to another with declining extrusion rate at a relatively constant dome height. (Melnik and Sparks, 1999)

99

DOME HEIGHT VS. EXTRUSION RATE
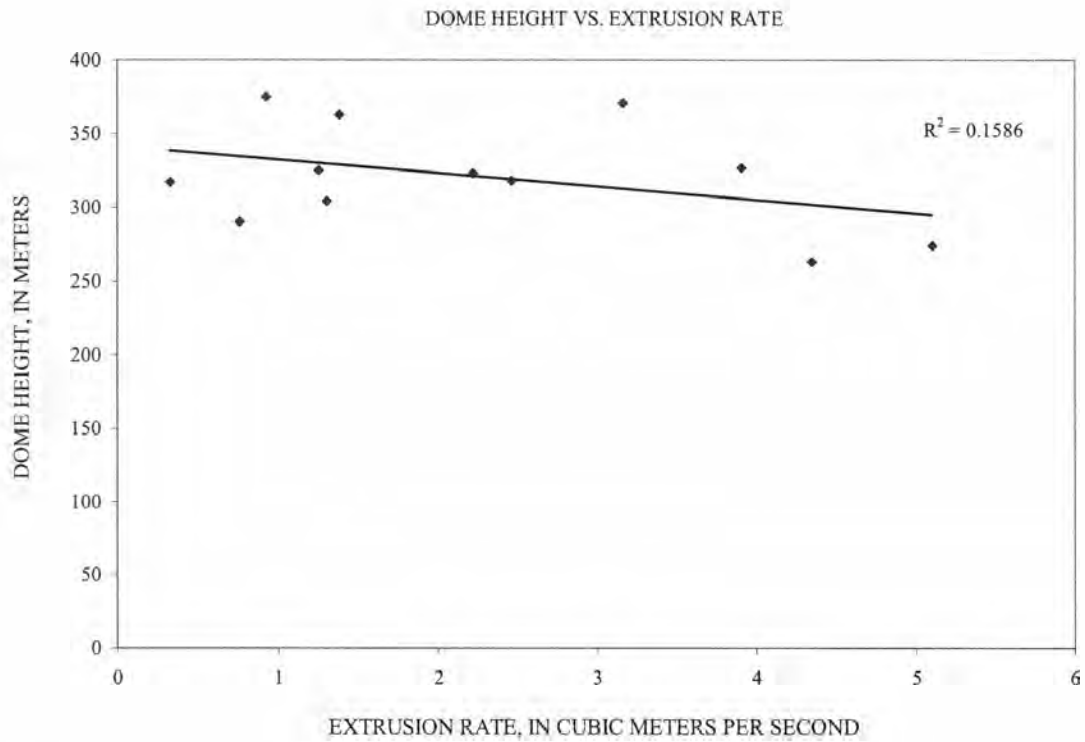
Figure 27. Direct relationship between dome height and extrusion rate (November 2004 – April 2007). The linear trend-line shows a weak inverse correlation between variables.
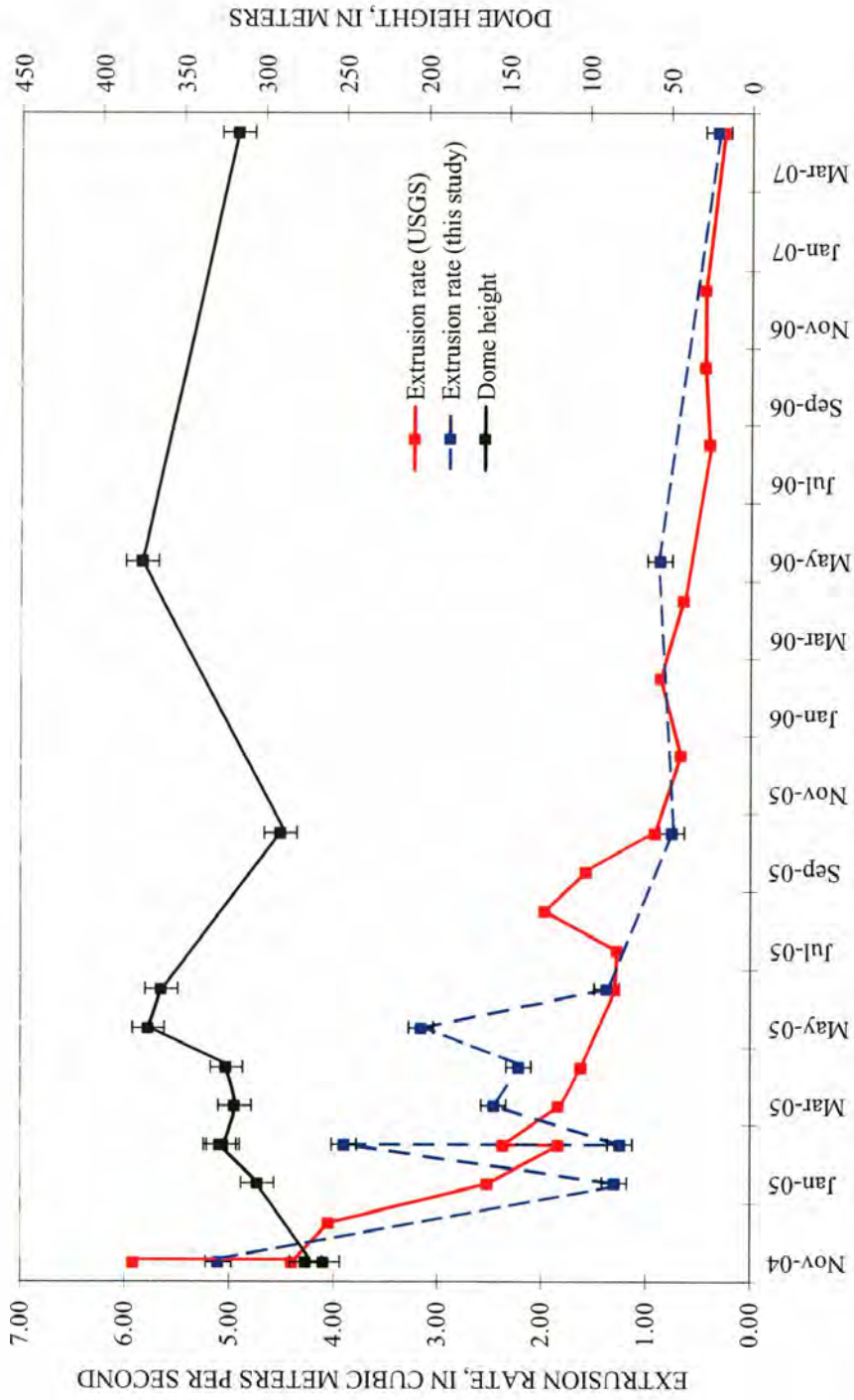
Figure 28. Dome height versus extrusion rates calculated by means of oblique photogrammetry and vertical aerophotogrammetry. Discrepancies between the estimated extrusion rate are attributed to missing dates (for both techniques) and uncertainties in volume estimates. In order to investigate the relationship between dome height and extrusion rate, comparison to estimates from both techniques is valuable. USGS extrusion rates provided by Schilling et al., *in press*.

101
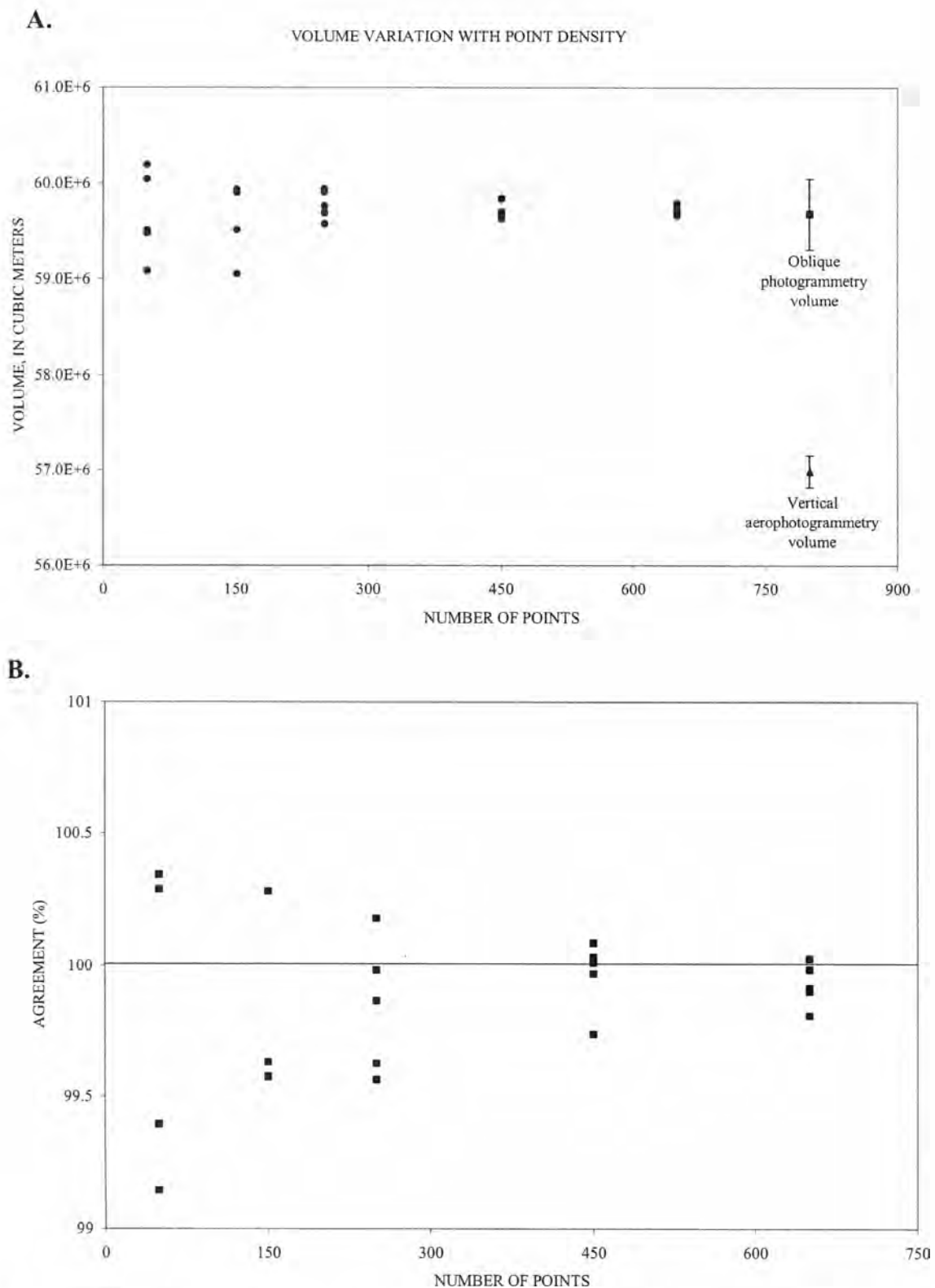
Figure 29. A. Volume variation with respect to number of points. The error bars represent volume estimate error based on a single date. **B.** Number of point subsets plotted against percent agreement to the ~800 point oblique DEM. Percent agreement deviations increase with a decrease in number of points used.

STANDARD DEVIATION VS. NUMBER OF POINTS
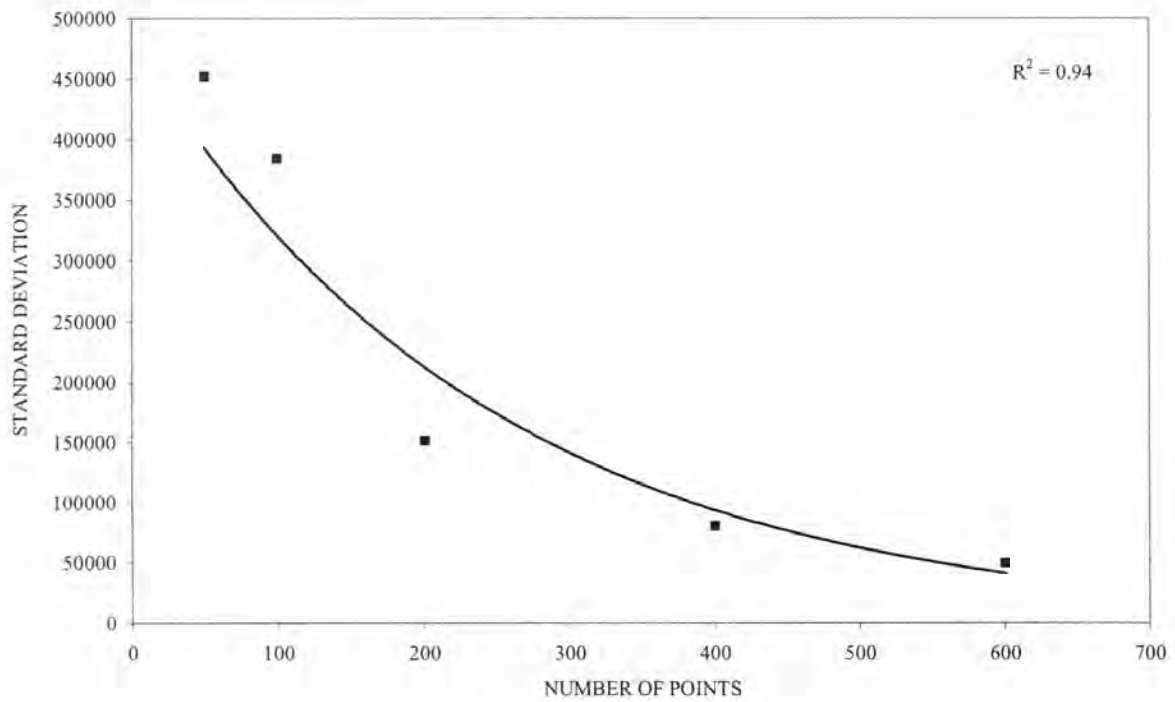
Figure 30. Standard deviation calculations of each subset of points (600, 400, 200, 100, 50). The trendline and associated R^2 value suggest an exponential relationship between the number of points and the precision of volume estimates.